

1 **Title:** CEP76 is a critical regulator of male germ cell transition zone function and tail composition

2

3 **Authors:** Brendan J. Houston^{1,*}, D. Jo Merriner¹, G. Gemma Stathatos¹, Anne E. O'Connor¹, Alexandra

4 M. Lopes^{2,3}, Donald F. Conrad⁴, Mark Baker⁵, Jessica E.M. Dunleavy¹, and Moira K. O'Bryan¹.

5

6 **Affiliations:**

7 ¹ School of BioSciences and Bio21 Institute, The University of Melbourne, Parkville, Australia

8 ² Instituto de Investigação e Inovação em Saúde, Universidade do Porto, Portugal

9 ³ Institute of Molecular Pathology & Immunology, University of Porto, Portugal

10 ⁴ Oregon National Primate Research Center, Oregon Health and Science University, Beaverton,

11 Oregon, USA

12 ⁵ School of Environmental and Life Sciences, The University of Newcastle, Callaghan, Australia

13

14 * **Corresponding author:** brendan.houston@unimelb.edu.au

15

16 **Running title:** CEP76 is a transition zone protein required for male fertility

17

18 **Keywords:** spermiogenesis, spermatogenesis, sperm motility, fibrous sheath, male infertility

19 **Abstract**

20 The transition zone is a specialised gate at the base of cilia/flagella, which segregates the ciliary
21 compartment from the cytoplasm and strictly regulates protein entry. In this study, we have identified
22 CEP76 as an essential germ cell transition zone protein, involved in the selective entry and
23 incorporation of key proteins required for sperm function and fertility into the ciliary compartment and
24 ultimately the sperm tail. In its absence sperm tails are shorter and immotile as a consequence of deficits
25 in essential sperm motility proteins including DNAH2 and AKAP4, which accumulate at the sperm neck
26 in the mutant. We demonstrate CEP76 is required for sperm tail fibrous sheath formation, outer dense
27 fibre loading and axoneme stability in the principal piece and ultimately sperm motility. Finally, we
28 identify that CEP76 dictates annulus positioning and composition, adding further evidence that the
29 spermatid transition zone and annulus are part of the same functional structure.

30

31 **Introduction**

32 Cilia and their organelle cousins, flagella, play essential roles in many cell types. Notably, a single
33 modified motile cilium (a flagellum) projects from male gametes and is essential for fertility in sexually
34 reproducing animals [1]. In eukaryotic cilia, the transition zone (TZ), also known as the ciliary gate, has
35 emerged as an essential mediator of cilia development through its role in controlling protein entry into
36 the ciliary compartment within which cilia/flagella develop [2-4]. The TZ develops immediately distal to
37 the mature centriole, from which the core of the cilia, the axoneme, develops. The TZ allows for the
38 selective transport of proteins into the cilium/flagellum and thus the establishment and maintenance of
39 a unique ciliary microenvironment [5, 6]. The TZ is largely composed of sheets of Y-shaped structures
40 that attach at one side to the developing axoneme, at a single point, and at the other side dock to the
41 plasma membrane, at two points [7, 8]. While TZ composition, including Y-shaped linkers, is poorly
42 understood, several genes that, when mutated, result in ciliopathies have been identified as core
43 members of the TZ [9-12]. To enact protein and vesicle transport across the TZ and along the
44 developing axoneme, cilia/flagella utilise a bi-directional transport process of intraflagellar transport (IFT)
45 with the aid of the BBSome [13, 14]. In addition, the distal appendages of the centriole (known as
46 transition fibres) play an essential role in protein trafficking into the ciliary compartment by acting as
47 docking sites for cargoes prior to their entry through the TZ [15].

48

49 The sperm tail is a modified motile cilium and while it is assumed that the formation of the TZ and core
50 of the axoneme will be similar to that which occurs in somatic cells, this is largely untested. Current
51 models of the TZ are largely informed by data from primary cilia, or the somatic flagella of lower order
52 species such as *Chlamydomonas* [16]. There is, however, emerging evidence to suggest differences in
53 TZ structure, composition and transport machinery exist to meet the demands of different cilia/flagella
54 sub-types (reviewed in [17]). As mammalian sperm contain accessory structures not seen in somatic
55 cells, it is reasonable to predict that the male germ cell TZ is modified to selectively recruit fibrous sheath
56 and outer dense fiber proteins into the ciliary lobe.

57

58 As with all motile cilia/flagella, sperm tail motility is dictated by the function of the axoneme – a 9+2
59 microtubule-based structure that runs the length of the tail [18, 19]. The sperm tail is composed of two
60 major sections: the midpiece, which houses the mitochondria; and the principal piece, wherein all
61 glycolytic enzymes are anchored to a structure called the fibrous sheath [20-23]. Both the midpiece and
62 principal piece compartments also contain outer dense fibres – which are circumferential to the
63 axoneme microtubules and act to protect the sperm tail from shearing forces [24, 25]. In the principal
64 piece, the longitudinal columns of the fibrous sheath replace the outer dense fibres 3 and 8 and are
65 linked by circumferential ribs [26, 27]. As per the axoneme, the outer dense fibres and fibrous sheath
66 are formed within the ciliary compartment and as such their component proteins must transition through
67 the TZ [24]. While this may suggest the requirement of additional factors to aid in the selective transport
68 of sperm-specific proteins via the TZ into the ciliary compartment, no such proteins of this function have
69 been identified.

70

71 In addition, towards the end of sperm tail development, the annulus, a septin-based ring that is thought
72 to be attached to, or physically a part of the TZ, migrates distally along the sperm tail to define the
73 junction of what will ultimately become the midpiece and principal pieces of the sperm tail [28, 29]. This
74 annulus is thought to be a diffusion barrier between the sub-compartments of the tail, and its loss is
75 often associated with a sharp bending at the midpiece-principal piece junction, poor sperm motility and
76 ultimately male infertility [28, 30]. At a similar time to annulus migration, but by a seemingly independent
77 process [28, 31, 32], the membrane attached to the basal body is pulled distally to the annulus, thus
78 exposing a portion of the axoneme (surrounded by the outer dense fibres) to the cytoplasm. This

79 process allows cytoplasmic mitochondria to be loaded onto the sperm tail to form the mitochondrial
80 sheath of the midpiece [24, 33].

81
82 Despite our descriptive understanding of a number of these processes, the mechanisms of sperm tail
83 development are still largely unknown. It is currently unclear how sperm-specific proteins, including
84 components of the accessory structures, are selectively transported via the TZ into the ciliary
85 compartment. In working to address this, we identified the previously unexplored centriole gene *CEP76*
86 as being essential for male fertility in men as highlighted by a missense mutation in an infertile man with
87 azoospermia (Figure S1; [34, 35]). *CEP76* has been suggested to play a role in centriole duplication in
88 somatic cell lines through interaction with the centriole protein CP110 [36, 37], but nothing was known
89 about its role in male fertility. *CEP76* expression is testis enriched [38] and *CEP76* has been localised
90 to centrioles in human spermatozoa and somatic cells [37, 39]. *CEP76* has two putative functional
91 domains (Figure S1): a C2 domain that is predicted to function in ciliary membrane targeting, and a
92 transglutaminase domain that is predicted to interact with tubulins in the axoneme or the TZ [40]. It is
93 hypothesised based on a large TZ protein comparative study, that these domains cooperate to play a
94 role in Y-shaped linker function (Zhang and Aravind, 2012) and likely TZ function. Thus, we aimed to
95 define the role *CEP76* plays in male fertility.

96
97 Within this study we identify *CEP76* as an essential male fertility gene, with a unique role in TZ function
98 and the selective entry of key motility proteins into the developing flagellum. Knockout males were
99 sterile and produced sperm with a variety of structural defects and the abnormal accumulation of key
100 proteins at the sperm neck, consistent with an inability to pass through the TZ during the process of tail
101 development. Consequently, formation of the mitochondrial sheath was significantly impaired in sperm
102 from *Cep76* knockouts. Collectively, these data identify *CEP76* as the first known germ cell-specific
103 regulator of transition zone function, which is required for male fertility in mammals.

104

105

106 **Results**

107 Cep76 is a spermatid enriched mRNA

108 Consistent with its putative role in male fertility, mouse *Cep76* is most highly expressed in the testis
109 (Figure S2A) with lower levels also detected in the brain. To define which germ cell types *Cep76* is
110 expressed in, we investigated its expression across the establishment of the first wave of mouse
111 spermatogenesis (Figure S2B). *Cep76* mouse testis expression levels were relatively consistent until
112 day 18 of age, and then notably increased at day 20 of age, coincident with the beginning of
113 spermiogenesis (first appearance of round spermatids). In agreement, single cell RNA sequencing of
114 mouse germ cells revealed that *Cep76* expression is considerably elevated in step 6-9 spermatids
115 (Figure S2C), at the time when the core of the sperm tail is formed. We tested multiple antibodies to
116 investigate CEP76 localisation in male germ cells but found all were non-specific (data not shown).

117

118 *Cep76* is required for male fertility in mice

119 To directly test the hypothesis that CEP76 is required for sperm tail development and thus male fertility,
120 we generated a knockout mouse model using CRISPR/Cas9 technology. We removed exon 3 of the
121 mouse gene (Figure S1E), which resulted in a premature stop codon in exon 4 of *Cep76*, which
122 produces one protein coding transcript (ENSMUST00000097542.3). This transcript encodes a protein
123 of identical length (659 AAs, predicted molecular mass of 74.3 kDa) and 97.7% identity (Figure S1B) to
124 the human *CEP76* principal isoform. Additionally, sequence comparison revealed that the amino acid
125 affected in the infertile man is a highly conserved residue from men to zebrafish (Figure S1B). *Cep76*
126 knockout was confirmed via qPCR (Figure S1F).

127

128 While knockout males were free of overt systemic disease and displayed normal mating behaviour, they
129 were sterile (Figure 1A). Knockout females were fertile (not shown). Body, testis, and epididymis
130 weights (Figures 1B, C and D) of *Cep76* knockout males were equivalent to wild type males. While the
131 daily sperm production of *Cep76* knockout males was similar to wild type counterparts (Figure 1E), the
132 number of sperm within their epididymides was reduced to approximately 35% of wild type levels (Figure
133 1F; $p < 0.0001$). The reduced sperm number in the *Cep76* knockout epididymis, in the absence of a
134 reduction in testis weight and daily sperm production was due to partial spermiation failure, as
135 evidenced histologically in stage IX tubules, wherein sperm were retained within the seminiferous
136 epithelium (Figure 1J). With the exception of spermiation failure, spermatogenesis appeared normal at

137 a light microscopic level in *Cep76* knockouts (Figure 1H). Similarly, epididymal histology was
138 comparable between genotypes (Figures 1K and L).

139

140 CEP76 is required for normal sperm morphology and motility

141 Analysis of sperm morphology via light microscopy revealed overt defects in sperm from knockout
142 males (Figure 2A). Total sperm tail and midpiece length (measured by mitochondrial sheath length) of
143 sperm from *Cep76* knockout males was significantly shorter (by 15% and 25%, respectively) than those
144 from wild type males (Figures 2B and C; $p < 0.0001$), suggesting a fundamental role of CEP76 in tail
145 assembly within the sperm ciliary compartment that is consistent with a role in TZ function and
146 mitochondrial loading. In agreement with the defects in sperm morphology, computer assisted sperm
147 analysis revealed a striking reduction in the percentage of sperm from knockouts displaying basic
148 twitching motility (Figure 2A; 6% in knockout versus 80% in wild type, $p < 0.0001$) and the virtual
149 absence of forward, progressively motile sperm in comparison to wild type males (Figure 2B; 0.4% in
150 knockout versus 42.4% in wild type, $p < 0.0001$). The small population of sperm from *Cep76* knockout
151 males that were classified as motile were seen to be simply twitching on the spot.

152

153 To examine the cause of the reduced mitochondrial sheath length in the absence CEP76, we measured
154 the distance between the base of the sperm head and the annulus as marked by SEPT4 staining (Figure
155 2F, G). Measurements revealed a significantly shorter distance between the annulus and nucleus in
156 sperm from *Cep76* knockout males relative to wild type (18.6 μm in knockout versus 22.6 μm in wild
157 type; $p < 0.0001$). In addition, the portion of sperm with SEPT4 positive staining (Figure 2H) was
158 significantly reduced in the absence of CEP76 (60% in knockout versus 84% in wild type, $p = 0.0095$),
159 suggesting poorly formed annuli.

160

161 Light microscopy and a visual examination also revealed defects in sperm head shape (Figure S3A) in
162 at least 40% of sperm from knockouts compared to 5% in wild type ($p < 0.0001$). We also observed a
163 significant increase in sperm with abnormal acrosomes from *Cep76* knockout males (35% in knockout
164 versus 3% in wild type, Figure S3D; $p < 0.0001$). In addition, we analysed sperm head morphology
165 using a nuclear shape analysis software. This revealed a significantly lower proportion of the knockout
166 population classified as normal (Cluster 1), while there were significant increases in sperm with slightly

167 (Cluster 2) and largely (Cluster 4) abnormal head shapes (compared to wild type). This analysis
168 revealed that ~70% of sperm heads from *Cep76* knockout males had abnormal nuclear morphology
169 (Figure S3E; $p < 0.0001$). In addition, there was a 2-fold increase in sperm decapitation in samples from
170 knockout males, indicating that the CEP76 plays a role in establishing patency of the head-tail coupling
171 apparatus (HTCA) (Figure S3C, $p < 0.0001$).

172

173 Collectively these results reveal CEP76 is required for the production and release of normal numbers
174 of functional sperm. Shorter sperm tails and annulus defects suggest CEP76 plays a role in TZ function.
175 Defects in nuclear morphology and a weakened HTCA are supportive of a role for CEP76 in manchette
176 function and/or acrosome formation and in the fortification of the neck region (a derivative of the basal
177 body) late in spermiogenesis. At a function level, sperm from *Cep76* knockout males are unable to reach
178 the site of fertilisation due to highly impaired sperm motility.

179

180 CEP76 is required for normal sperm flagella and HTCA ultrastructure

181 In order to define the origins of the motility and structural defects, we investigated sperm ultrastructure
182 using transmission (TEM) and scanning electron microscopy (SEM) on isolated epididymal sperm
183 (Figures 3, 4, Figure S4). At the midpiece level, the axoneme ultrastructure appeared superficially
184 normal, bearing all outer dense fibres and the 9+2 microtubule formation with dynein arms in sperm
185 from wild type and knockout males (Figure 3A, B, respectively). In *Cep76* knockout sperm, however, a
186 build-up of mitochondria, and membranes was seen at midpiece level cross-sections (Figure 3C).
187 Longitudinal sperm tail sections of the midpiece from knockout males additionally revealed abnormal
188 mitochondria with enlarged spacing within mitochondrial matrixes (Figure 3H) and notable mitochondria
189 aggregation (Figure 3I – arrow).

190

191 Investigation of the axoneme ultrastructure at the principal piece level revealed absent outer dense
192 fibres and microtubule doublets in many sperm tails from knockout males (Figure 3D-F), suggesting
193 this compromise, which was absent at the midpiece level, may have been influenced by fibrous sheath
194 assembly. In addition, we observed the abnormal formation of the annulus, again suggesting an origin
195 of poor TZ formation. Specifically, in sperm from *Cep76* knockout males the annulus was not clearly
196 distinguishable from the fibrous sheath (Figure 3K), or not identifiable (Figure 3L). In addition, we

197 observed rare examples of mitochondria incorporated within the principal piece in *Cep76* knockout male
198 sperm (Figure 3K), but never in sperm from wild type controls.

199
200 Examination of the sperm neck region by TEM (Figure S4D-F) revealed a number of abnormal
201 structures, including imperfect capitulum structures and a build-up of mitochondria and ectopic vesicles
202 in sperm from *Cep76* knockout males. Further, an excess of what we predicted to be granulated bodies
203 was seen throughout the cytoplasm (Figure S4E). Granulated bodies are transported into the ciliary
204 compartment to form the outer dense fibres which is continuous with the HTCA [42]. This finding
205 strongly supports a role for CEP76 in the selective entry of proteins and vesicles into the ciliary
206 compartment during spermiogenesis and, by extension, in building of the ODF and the fortification of
207 the HTCA. Of relevance, we did not observe a significant difference in the proportion of sperm positive
208 for SUN5 staining, a protein required for the fortification between the capitulum and basal plate [43],
209 between genotypes, i.e., the junction with the nuclear membrane (Figure 2I; $p = 0.26$). As this structure
210 is proximal to where the TZ exists, this data is consistent with a role for CEP76 in the TZ and the
211 assembly of more distal regions of the tail.

212
213 CEP76 is required for the assembly of sperm tail accessory structures and annulus migration
214 *Annulus*
215 Scanning electron microscopy of sperm from *Cep76* knockout males further emphasised the poorly
216 formed annulus and accessory structures in the midpiece and principal piece (Figure 4). In sperm from
217 wild type males, the annulus was appropriately positioned at the junction between the mitochondrial
218 sheath of the midpiece and the fibrous sheath of the principal piece (Figure 4A, D). In sperm from *Cep76*
219 knockout males, while the annulus was often associated with the fibrous sheath, it was rarely found
220 aligned at the distal border of the mitochondrial sheath (Figure 4B, C, E, F). As a result, a region of
221 exposed ODFs was evident between the mitochondrial sheath and the annulus or fibrous sheath.
222 Quantification of the defects in annulus positioning (Figure 4M) revealed a normal positioning and
223 structure of the annulus in only 10% of sperm from knockouts males compared to 95% of sperm from
224 wild type males ($p = 0.0002$). Consequently, we quantified the incidence of ODF-exposed regions at
225 the distal midpiece (Figure 4N). This revealed that ODFs were exposed in 97% of sperm from *Cep76*
226 knockouts but only 10% of sperm from wild type ($p = 0.0002$). In many cases, the annulus was found

227 embedded within the proximal region of the fibrous sheath (e.g., Figure 4K) rather than at the junction
228 of the midpiece, or it was not clearly observed due to large deformations in the fibrous sheath (Figure
229 4F). Due to the predicted role of CEP76 in TZ function, we anticipate this is due to a defect in TZ/annulus
230 migration rather than the fibrous sheath assembling too far proximally.

231

232 *Mitochondria*

233 As above, mitochondrial packing in epididymal sperm from *Cep76* knockouts was irregular and
234 characterised by misaligned and poorly compacted mitochondria along the mitochondrial sheath (Figure
235 4H versus 5G). Mitochondrial aggregation defects identified via TEM were confirmed via SEM and were
236 characterised by collections of poorly formed mitochondria and a build-up around the midpiece (Figure
237 4I). Scoring of mitochondrial sheath normality (as defined in the methods; Figure 4O) revealed a
238 significant reduction in quality in sperm from *Cep76* knockout males compared to wild type (3.5 in
239 knockout versus 4.6 in wild type; $p < 0.0001$).

240

241 *Fibrous sheath*

242 Finally, SEM revealed that fibrous sheath formation was notably impaired in the absence of CEP76
243 (Figures 4C, F, K, L). In wild type sperm, the fibrous sheath is comprised of two longitudinal columns
244 linked by circumferential ribs. Gaps in the fibrous sheath were evident at regular intervals (Figure 4D,
245 J). In the absence of CEP76, however, gaps/slits between circumferential ribs were rare (Figure 4K)
246 and in many cases the ribs appeared to be unanchored and projected from the body of the tail (Figure
247 4L). Notably, the proximal portion of the fibrous sheath appeared to be the most disorganised (e.g.,
248 Figure 4C). Fibrous sheath normality was scored (as detailed in the methods; Figure 4P), revealed a
249 highly significant reduction in fibrous sheath quality in sperm from *Cep76* knockouts (1.6 in knockout
250 versus 2.9 in wild type; $p < 0.0001$).

251

252 Collectively, these data reveal CEP76 is a key determinant in the development of multiple aspects of
253 sperm tail development, including the fibrous sheath, annulus, and positioning and the mitochondrial
254 sheath.

255

256 Loss of CEP76 leads to aberrant sperm composition

257 To explore the hypothesis that CEP76 is involved in the selective entry of proteins into the ciliary lobe
258 at a molecular level, we performed quantitative mass spectrometry on sperm from the cauda epididymis
259 of *Cep76* knockout and wild type males (Table 1A). Doing so identified 32 differentially expressed
260 proteins in sperm from knockout males (13 up-regulated and 19 down-regulated), including multiple
261 mitochondrial and apoptotic proteins. This difference in mitochondrial protein content is consistent with
262 the abnormal accumulation of mitochondria around the sperm tail as detailed above. In agreement with
263 the observed reduced tail length, alpha tubulin content was significantly reduced in sperm from *Cep76*
264 knockout males. In a separate analysis, and to account for differences in tail length, the content of
265 known (or predicted) sperm tail proteins was normalised to alpha tubulin. As shown in Table 1B,
266 following this normalisation, 14 proteins were identified as significantly altered in sperm from *Cep76*
267 knockout males compared to wild type including several that are essential for sperm tail function and
268 male fertility. They included: axonemal protein DNAH2 (1.65-fold wild type levels, $p = 0.0406$), the actin-
269 based motor protein myosin 9 (3.5-fold wild type levels, $p = 0.0174$) and AKAP3 and AKAP4, which are
270 major components of the fibrous sheath [22] (1.36-fold and 1.46-fold wild type levels, $p = 0.032$ and p
271 = 0.0498, respectively).

272
273 To investigate this counterintuitive increase in several motility proteins, we defined the localisation of
274 DNAH2 and AKAP4 proteins in sperm from *Cep76* knockout males using immunofluorescence (Figure
275 5). As expected, in wild type sperm, the dynein arm protein DNAH2 was uniformly localised throughout
276 the midpiece and principal piece of the tail (Figure 5A) [44, 45]. In contrast, while DNAH2 was found
277 within the sperm tail in many sperm from *Cep76* knockouts, it was notably accumulated in the neck
278 region. In other sperm, DNAH2 was seen nearly exclusively localised to the neck and appeared to be
279 almost absent from the tail (Figure 5A). Specifically, 22% of sperm from *Cep76* knockout males
280 displayed an accumulation of DNAH2 in the neck region compared to 5.1% of sperm from wild types
281 (4.3 x wild type levels, $p = 0.0006$; Figure 5C). Tail pixel intensity analysis (per area) revealed a 25%
282 reduction in DNAH2 content across the entire flagellum ($p < 0.05$; Figure 5E).

283
284 Also as expected for a component of the fibrous sheath, AKAP4 was primarily localised to the principal
285 piece sperm from wild type (Figure 5B). As above, in *Cep76* knockout sperm, AKAP4 accumulated in
286 the neck region in 13% of sperm compared to 4% in sperm from wild type mice (Figure 5D).

287 Quantification of neck AKAP4 staining revealed 3.1-fold levels in *Cep76* knockout sperm relative to wild
288 type (Figure 5D). An analysis of pixel intensity revealed a significant, 40% reduction in AKAP4 content
289 (per area) within the principal piece of sperm from *Cep76* knockout males compared to wild type ($p <$
290 0.0001; Figure 5F).

291
292 Collectively, these data underscore an essential role for CEP76 in TZ function and the regulated entry
293 of key sperm tail proteins into the ciliary compartment and sperm tail development.

294
295 CEP76 is not required for manchette formation and migration
296 SEM confirmed the magnitude of head deformation in sperm from *Cep76* knockout males (Figure S4A-
297 C). The manchette is critically involved in shaping the proximal half of the sperm nucleus and further
298 acts as a transport freeway for protein delivery to the basal body and into the sperm tail [24]. Despite
299 the highly irregular sperm head shape, the formation of the manchette appeared normal in the absence
300 of CEP76 as identified by alpha tubulin staining of isolated germ cells (not shown) and testis sections
301 (Figure S3F). Electron microscopy reinforced that manchette structure was overtly normal (not shown).

302
303 CEP76 is required for the maintenance of centriole number in male germ cells
304 CEP76 has previously been linked to a role in the suppression of centriole duplication in 293T cells [37],
305 thus raising the possibility of a similar role in germ cells. To explore this hypothesis, we stained purified
306 round and elongating spermatids with the centriole marker centrin (Figure S6G, H) and quantified the
307 number of centrioles per cells (Figure S6I). As expected, two distinct centrin foci were observed in 84%
308 of wild type spermatids and only 1% of wild type cells exhibited 3+ centrin foci. By contrast, in
309 spermatids from *Cep76* knockout males, 18% of cells possessed 3 or more centrioles structures ($p =$
310 0.0002) and only 70% of cells contained 2 centrin foci ($p = 0.0012$). These data confirm a role for CEP76
311 in germ cell centriole duplication suppression. Despite this finding, sperm from *Cep76* knockouts
312 contained only single tails, i.e., centriole overduplication did not lead to multiple basal bodies and
313 axoneme growth.

314
315 **Discussion**

316 Building a sperm tail is a complex and multistep process, requiring the coordinated action of multiple
317 protein and organelle transport processes (reviewed in [24, 46]), and is absolutely essential for male
318 fertility. The spermatid centriole is inherited during the process of meiosis. It subsequently duplicates
319 and matures to give rise to the basal body that docks to both the plasma and nuclear membranes [47,
320 48]. From this structure, the sperm tail, a modified cilium, forms through the selective entry of proteins
321 into the ciliary compartment via the TZ that sits at the junction between the cytoplasm and the ciliary
322 compartment. Assuming that cilia formation during germ cell development is analogous to primary cilia
323 wherein TZ function has been studied, all component proteins for the axoneme, outer dense fibers and
324 fibrous sheath must be selectively transported through the TZ. In this study, we establish CEP76 as the
325 first protein shown to play a male germ cell specific role in the TZ and demonstrate that CEP76 is
326 required for the development of functionally competent sperm. We show CEP76 is essential for the
327 efficient transport of AKAP4 proteins into the flagella compartment, underpinning normal fibrous sheath
328 development. We also show that it facilitates the incorporation of tubulin into the tail, and that an
329 absence of CEP76 leads to short sperm tails. Equally, it optimises the entry of DNAH2, a core
330 component of the axoneme motility apparatus. In the absence of CEP76, the sperm axoneme is
331 functionally incompetent. Following development of the core axoneme, CEP76 is required for
332 positioning of the annulus and thus influences mitochondrial sheath length. In addition to its TZ function,
333 our data reveal that analogous to its roles in somatic cells [37], CEP76 plays a role in the suppression
334 of centriole duplication in haploid male germ cells. This study highlights *CEP76* as a bona fide male
335 fertility gene in men and mice and adds to the growing evidence that several genetic factors contribute
336 to both sperm morphology and sperm count.

337

338 It has recently been suggested that the annulus and TZ are part of the same ciliary structure [29] and
339 our data support this idea. The annulus shares a number of proteins with the TZ and the localisation of
340 several of these proteins (e.g., CEP290, MKS1) follows annulus migration during late spermiogenesis
341 [49]. Consistent with this, the abnormal annulus structures observed in sperm from *Cep76* knockout
342 males suggests that TZ structure influences annulus structure and function. Specifically, we show that
343 CEP76 is required for annulus positioning, and, in its absence, the annulus is poorly formed and
344 migrates a shorter distance. Very little is known about factors that govern annulus migration and
345 positioning [50], but these processes do not appear to be influenced by development of the fibrous

346 sheath that ultimately borders the annulus in mature spermatids but is formed prior to annulus migration.
347 This is highlighted by data from *Akap3* and *Akap4* knockout mice, which exhibit poor sperm fibrous
348 sheath development, annulus positioning and midpiece length [20, 30, 51]. Equally, the absence of an
349 annulus in *Sept4* and *12* mutant models did not impair fibrous sheath formation [28, 32].

350
351 It has been hypothesised that within CEP76 the C2 and transglutaminase domains cooperate to allow
352 CEP76 to play a role in the transition zone as a Y-shaped linker [40]. Y-shape linker structures form the
353 main body of the TZ; proteins of which can be grouped into the Meckel syndrome (MKS) and
354 nephronophthisis (NPHP) complexes [52]. These complexes participate in multiple roles during
355 ciliogenesis – TZ attachment, core axoneme extension and then regulation of components entry into
356 the cilia/flagella [53]. Based on domain architecture and functional predictions, CEP76 has been
357 hypothesised to span both MKS and NPHP complexes [40]. The presence of a C2 domain in CEP76
358 strongly suggests it anchors at the side of the Y-shaped linker interacting with the plasma membrane
359 [40]. Our data highlight that, *in vivo*, CEP76 is not essential for axoneme formation, for example
360 compared to CEP290, where CEP290 absence precludes TZ formation and ciliogenesis altogether [54,
361 55]. Rather, data suggest that CEP76 plays a facilitative role in TZ function specifically in male germ
362 cells and is likely not a core Y-linker component. As mice did not show symptoms of MKS or NPHP, our
363 data reveal CEP76 is not essential for somatic cells TZ function. The possibility exists, however, that
364 mice possessed subtle defects in somatic tissues.

365
366 Further, our proteomics results revealed the content of only a small number of sperm tail were altered
367 in the absence of CEP76, supporting the hypothesis that CEP76 is highly selective in its function and
368 that other TZ proteins are required to form a functioning sperm tail. This is consistent with the concept
369 that TZ content is cell type-specific and that different TZ proteins are involved in the selective
370 recruitment of precise subsets of proteins from the many thousands of proteins present with the cell
371 cytoplasm, i.e., the TZ functions as a cell type-specific filter controlling entry into cilia.

372
373 Overt consequences of CEP76 loss included the abnormal assembly and content of sperm tail
374 accessory structures. We observed inappropriate packaging of the fibrous sheath and the absence of
375 spacing between the circumferential ribs. AKAP4 is the most abundant fibrous sheath protein,

376 constituting nearly half its entire content [56], and acts as a scaffold protein for both the longitudinal
377 columns and ribs, while AKAP3 plays a similar role in the ribs of the fibrous sheath [21, 57]. The fibrous
378 sheath defects seen in the absence of CEP76 are consistent with the poor entry of major fibrous sheath
379 proteins into the sperm tail compartment via the TZ. Similarly, we identified an accumulation of
380 granulated bodies in the sperm neck region and the partial absence of outer dense fibres in the principal
381 piece axoneme. Collectively, our results strongly suggest the deficit in the entry of fibrous sheath and
382 outer dense fibre components into the tail compartment limited the normal formation of accessory
383 structures and thus directly impaired sperm motility.

384

385 Finally, we identified significant aggregation of mitochondria and morphology in the midpiece. The
386 mitochondrial sheath is the last accessory structure to be loaded onto the sperm tail. This occurs in
387 parallel with the migration of the annulus and plasma membrane down to a position immediately
388 proximal, and abutting, the principal piece, as marked by the start of the fibrous sheath, [24, 58].
389 Although the membrane migration occurs at the same time as annulus migration, it does not appear to
390 be driven by the annulus as the former occurs even when the annulus does not form [28, 30]. While the
391 annulus is not required for mitochondrial sheath formation, in its absence mitochondrial morphology is
392 frequently abnormal [28, 31, 59]. Prior to their loading, spherical mitochondria are recruited from the
393 cytoplasm and ordered in four columns parallel to the axoneme. They then move towards the core of
394 the tail and attach to the outer dense fibers, elongate, coil and stagger, to intercalate around the
395 midpiece [58]. Next, mitochondria elongate and attach end-to-end to form a double helix around the
396 axoneme. *Cep76* knockout sperm mitochondria were largely elongated and uniform along the midpiece,
397 suggesting that mitochondrial recruitment and early mitochondrial elongation processes proceeded
398 normally. We predict the shorter annulus migration distance in sperm from *Cep76* knockout males
399 leaves insufficient space for the normal number of mitochondria to coil around the sperm tail, i.e.
400 sterically interfere with the later processes of mitochondrial elongation and prevent their tight
401 compaction within the midpiece [60]. Ultimately, the patency of the annulus to act as a barrier between
402 major sperm tail compartments also likely influenced the loading of mitochondria, as demonstrated by
403 examples of mitochondria in the principal piece section.

404

405 Our data revealed a second function of CEP76 in male germ cells – a role in supressing supernumerary
406 centrioles, analogous to its role identified in human sarcoma cells *in vitro* [37]. A previously established
407 mechanism highlighted that CEP76 controls centriole duplication via interaction with PLK1 and CP110
408 [36, 37]. While not investigated directly here, we note *Cep76* knockout mice were viable and were free
409 of any overt body wide disease, suggesting that CEP76 is not essential for centriole function in somatic
410 tissues.

411
412 To the best of our knowledge, this is the first example of a protein with a germ cell-specific function in
413 the TZ. In the absence of CEP76, essential components of the sperm tail are unable to enter the ciliary
414 lobe, meaning less or minimal incorporation into the growing tail and thus male infertility. These data
415 provide support for the concept that TZ composition is cell type-specific and that the TZ provides an
416 additional layer of specificity to the composition and function of cilia and flagella.

417
418 **Materials and methods**
419 Ethics statement
420 Experimental procedures involving mice followed animal ethics guidelines generated by the Australian
421 National Health and Medical Research Council (NHMRC). All animal experiments were approved by
422 the Animal Experimentation Ethics Committee (BSCI/2017/31) at Monash University, or The University
423 of Melbourne Animal Ethics Committee (application 20640).

424
425 Knockout mouse production
426 As described previously [34], exome sequencing of infertile men identified *CEP76* as a high confidence
427 candidate male fertility gene. The patient carried a homozygous c.607G>C (p.Gly203Arg) missense
428 variant in a conserved residue of *CEP76*, which was predicted to be intolerant to variation (Figure S1).
429 Pathogenicity assessments using SIFT and Polyphen-2 [61, 62] predicted the missense variant to affect
430 function (SIFT) and to be possibly damaging (Polyphen). To test the requirement for CEP76 in male
431 fertility, *Cep76* knockout mice were generated on the C57BL/6J background through the Monash
432 University Genome Modification Platform (a partner of the Australian Phenomics Network) using
433 CRISPR/Cas9 technology. Excision of exon 3 of *Cep76* was undertaken with CRISPR guide sequences
434 targeting regions flanking exon 3: upstream – TTTAAACTCAGTTCGTGGT and downstream –

435 GGTCTACATAGTAAAGTTCT. This was predicted to lead to a premature stop codon in exon 4 and a
436 truncated protein in the only protein-coding transcript of *Cep76* (ENSMUST00000097542.3). Changes
437 in gene sequence were identified with Sanger sequencing. Mice heterozygous for the *Cep76* deletion
438 were intercrossed to generate knockout individuals and wild type controls. Genotyping was performed
439 by Transnetyx (Corvoda, USA) using the primers F – CCCATTAACAGCCTCTGCTTCATAA and R –
440 GAGACAGGGTTCTCTGTGAATTCT. A reduction in *Cep76* transcript level (primers F –
441 GCGGCTCGATTGTTAATGT and R – AGTCCCCACACAGACAAAGG), was verified via qPCR on
442 testis cDNA relative to *Ppia* (primers F – CAGTGCTCAGAGCTCGAAAGTTT and R –
443 ACCCTGGACATGAATCCT).

444

445 CEP76 species alignments

446 CEP76 protein alignments were conducted using the protein Basic Local Alignment Search Tool (NCBI).
447 Sequences used were *Homo sapiens* ENSP0000262127; *Pan troglodytes* ENSPTRP00000016812;
448 *Macaca mulatta* ENSMMUP00000069818; *Rattus norvegicus* ENSRNOP00000034590; *Mus musculus*
449 ENSMUSP00000095149; *Danio rerio* ENSDARP00000075595. We compared entire protein identity across
450 species and focused on the conservation of amino acid 203G, which was mutated in the infertile patient
451 (Figure S1B).

452

453 Analysis of *Cep76* expression

454 Whole organ RNA was extracted from adult mouse brain, epididymis, heart, liver, lung, spleen and
455 testis, as well as testes from mice aged day 0-50, to investigate the expression of *Cep76* across different
456 tissues and throughout the establishment of the first wave of spermatogenesis. Each tissue was
457 homogenized in TRIzol Reagent to isolate RNA, which was converted to cDNA and used for qPCR with
458 SYBR Green master mix as previously described [63]. Primers used to detect *Cep76* were F –
459 CTCGGTCACCAGCAATGAAA and R – CAGACAGTGGTGAGGCCAAG, and housekeeping gene
460 *Ppia* are denoted above. We also utilised single cell RNA sequencing data contained within
461 FertilityOnline (<https://mcg.ustc.edu.cn/bsc/spermgenes2.0/index.html>) to investigate *Cep76*
462 expression in mouse testes.

463

464 Fertility analysis

465 Knockout males (*Cep76*^{-/-}) and wild type male littermates (*Cep76*^{+/+}) were aged to 10-14 weeks and
466 their fertility was assessed using the pipeline outlined previously [64]. In brief, 5 mice of each genotype
467 were setup to mate with 2 independent wild type females each (6-12 weeks old). The presence of a
468 copulatory plug was recorded as an indication of successful mating. Litter sizes were recorded as the
469 number of pups generated per plug. Males were subsequently culled and weighed (10-14 weeks of
470 age), and one testis and epididymis were dissected and processed for histological assessment.
471 Additional testes and epididymides were snap frozen on dry ice for calculation of daily sperm production
472 and epididymal sperm counts as described previously [65]. In addition, sperm were collected from the
473 cauda of the epididymis through backflushing, then resuspended in MT6 medium at 37°C for motility
474 assessment via computer assisted semen analysis [66]. Residual sperm were washed in PBS then
475 dried onto SuperFrost slides overnight. Sperm were then fixed in 4% paraformaldehyde for 10 min and
476 washed in PBS and stained with Mayer's haematoxylin for 10 min and eosin (Amber Scientific, Midvale,
477 Australia) for 1 min to allow an assessment of sperm morphology and tail length. Alternatively, fixed
478 sperm were permeabilized in 0.1% Triton-X-100/PBS (Sigma Aldrich, Castle Hill, Australia) for 10 min,
479 washed in PBS and stained with 10 µg/ml DAPI (ThermoFisher Scientific, Scoresby, Australia) to allow
480 an assessment of sperm head morphology, or 1 µg/ml peanut agglutinin conjugated to AlexaFluor-488
481 to label the acrosome. Head morphology assessment was performed using Nuclear Morphology
482 Analysis software version 1.17.1 [67] via an ImageJ plugin (National Institutes of Health, USA). All
483 length measurements (midpiece length, tail length and annulus positioning) were measured using
484 ImageJ (version 1.52k).

485

486 Electron microscopy

487 To investigate germ cell ultrastructure, testes were processed for electron microscopy as outlined
488 previously [68]. Similarly, caudal sperm were backflushed into MT6 medium and processed for electron
489 microscopy as outlined previously [68]. Images were taken either on a Jeol 1400 Plus electron
490 microscope at the Vera and Clive Ramaciotti Centre for Electron Microscopy (Monash University,
491 Australia), or a Talos L120C or a FEI Teneo VolumeScope at the Ian Holmes Imaging Center (The
492 University of Melbourne). To view the mitochondria, annulus, and fibrous sheath structure of sperm via
493 SEM, sperm were isolated from the cauda epididymis and incubated in 100 µl of 1 x PBS for 30 min to
494 strip the plasma membrane then processed as outlined in [69].

495

496 Scoring of mitochondrial sheath, fibrous sheath and annulus normality

497 To quantify the degree of ultrastructural defects within sperm tail structures, scoring of each structure
498 (mitochondrial sheath, fibrous sheath, and annulus) was performed on SEM images. For each biological
499 replicate, ten sperm were assessed. Mitochondrial sheath normality was scored 1-5: 1 – missing
500 mitochondria; 2 – many abnormally oriented and/or thick mitochondria; 3 – few abnormally oriented
501 and/or thick mitochondria; 4 – broadly normal with very few abnormally oriented mitochondria; 5 – no
502 defects where ‘normal’ was defined as homogeneously coiled mitochondria, with none missing, thick or
503 abnormally oriented. Fibrous sheath normality was score from ranks 1-3: 1 – no slits and/or massive
504 aggregation of circumferential ribs or longitudinal columns; 2 – reduced number of slits or slight
505 aggregation; 3 – normal structure, where normal was defined as slits occurring at regular intervals and
506 no aggregation. Annulus normality was score as: normal – intact, not shrunken, and localised to the
507 junction between the midpiece and principal piece; or abnormal – small, ectopically placed or
508 unidentifiable.

509

510 Mass spectrometry to define sperm protein composition

511 Sperm were backflushed from caudae epididymides of adult wild type (1 mouse per replicate, $n = 3$
512 replicates) and *Cep76* knockout males (2 mice per replicate due to reduction in epididymal sperm
513 content) into MT6 medium for 15 min at 37°C. Sperm were washed three times in 1 x Tris buffered
514 saline, pelleted, and then stored at -80°C. Sperm pellets were then dried in a speed vacuum and
515 prepared for liquid chromatography tandem mass spectrometry and run on a SCIEX QTRAP6500 as
516 described previously [70].

517

518 Data were assessed as 1) total/raw spectral counts or 2) total spectral counts were normalised to the
519 alpha tubulin content (alpha tubulin chain 8) for a comparison of sperm tail protein content in recognition
520 of the shorter sperm tails measured from *Cep76* null mice. Sperm tail proteins were identified via
521 proteomics or localisation studies. For completeness, proteins with an unknown localisation or that are
522 localised throughout the head and tail were included in the tail protein group. Proteins associated
523 exclusively with the sperm head or neck and mitochondrial proteins were not included here as the
524 normalisation process (to alpha tubulin) as they are not core sperm tail proteins. A two-tail t-test was

525 used to determine significant differences in protein content between genotypes. All data are available
526 in Table S1.

527

528 Immunofluorescence and protein localisation

529 To define centriole number in male germ cells, spermatids were isolated from the testes of males using
530 the STAPUT method [71]. Cells were settled onto poly-L-lysine coated SuperFrost slides for 15 min and
531 then fixed in ice cold methanol at -20 °C for a maximum of 7 min. Slides were immediately washed and
532 rehydrated in PBS. Fixed spermatids were permeabilised in 0.2% Triton-X-100/PBS for 10 min, blocked
533 in CAS-block (Dako), incubated overnight in 0.1 µg/ml Centrin antibody (Merck 04-1624) to stain
534 centriole components and beta tubulin (Abcam ab21057) to stain the manchette for spermatid staging,
535 then counterstained with DAPI. Z-stacks were taken using a Leica SP8 confocal and flattened to capture
536 all slices in a single frame. The number of centriole components per spermatid was then counted for
537 100 cells per replicate, per genotype.

538

539 To define the localisation of a sub-set of differentially expressed proteins, fixed sperm were
540 permeabilised in 0.2% Triton-X-100/PBS, blocked in CAS-block, incubated overnight in primary
541 antibodies (0.5 µg/ml DNAH2 [Invitrogen 64309], 2.5 µg/ml SEPT4 [Abcam 166788]) at 4 °C, stained
542 with relevant fluorescent secondary antibodies (ThermoFisher Scientific) for 1 h, then counterstained
543 with DAPI. For other antibodies (2.8 µg/ml AKAP4 [ProteinTech 24986-1-AP], 0.8 µg/ml SUN5
544 [ProteinTech 17495-1-AP]) sperm were permeabilised in 0.5% Triton-X-100/PBS. For the assessment
545 of sperm mitochondrial sheath length, live sperm were loaded with 5 µM Mitotracker Red CMXRos in
546 MT6 solution for 30 min as per the manufacturer's instructions. Sperm were then washed in PBS, fixed
547 in 4% paraformaldehyde and allowed to settle onto slides, as described above. All images were taken
548 using cellSens software (Olympus, Notting Hill, Australia) on an Olympus BX-53 microscope (Olympus)
549 equipped with an Olympus 392 DP80 camera or a Leica SP8 confocal. Immunofluorescence staining
550 intensity was used as a surrogate of protein content in sperm tails. FIJI v2.1.0 was used to trace sperm
551 tails (freehand line tool) and measure the average pixel intensity for AKAP4 and DNAH2 staining, to
552 account for differences in tail length.

553

554 CEP76 localisation in testis sections, germ cells and sperm was attempted with two antibodies: Abcam
555 ab86613 and Bethyl #A302-326A. Both antibodies reacted with antigens in knockout tissue.

556

557 **Statistical analysis**

558 Statistical analyses to determine significance between wild type and *Cep76* knockout data were
559 performed in Prism 9 (GraphPad, San Diego, USA) using a student's t-test on average data per mouse.
560 A nested t-test was used to analyse sperm midpiece length, sperm tail length, annulus migration
561 distance, mitochondrial sheath and fibrous sheath ultrastructure score, and pixel intensity analysis of
562 protein entry in the sperm tail. In these datasets, multiple sperm were measured or assessed within a
563 single biological replicate and each data point was used. A p value less than 0.05 was considered
564 significant.

565

566 **Funding**

567 This work was supported by a National Health and Medical Research Council grant awarded to MKOB
568 (APP1120356).

569

570 **Author roles**

571 BH, AEOC, JM, GS, JD and MB undertook experiments.

572 BH, GS and MKOB analysed data.

573 BH, JD and MKOB designed the experiments and wrote the paper.

574 All authors provided intellectual input and feedback on drafts.

575 All authors reviewed and approved the final publication.

576

577 **References**

- 578 1. Inaba, K., *Sperm flagella: comparative and phylogenetic perspectives of protein components*.
579 Mol Hum Reprod, 2011. **17**(8): p. 524-38.
- 580 2. Garcia-Gonzalo, F.R., et al., *A transition zone complex regulates mammalian ciliogenesis and*
581 *ciliary membrane composition*. Nat Genet, 2011. **43**(8): p. 776-84.
- 582 3. Hu, Q., et al., *A septin diffusion barrier at the base of the primary cilium maintains ciliary*
583 *membrane protein distribution*. Science, 2010. **329**(5990): p. 436-9.
- 584 4. Chih, B., et al., *A ciliopathy complex at the transition zone protects the cilia as a privileged*
585 *membrane domain*. Nat Cell Biol, 2011. **14**(1): p. 61-72.
- 586 5. Goncalves, J. and L. Pelletier, *The Ciliary Transition Zone: Finding the Pieces and Assembling*
587 *the Gate*. Mol Cells, 2017. **40**(4): p. 243-253.
- 588 6. Nachury, M.V., E.S. Seeley, and H. Jin, *Trafficking to the ciliary membrane: how to get across*
589 *the periciliary diffusion barrier?* Annu Rev Cell Dev Biol, 2010. **26**: p. 59-87.

- 590 7. Arima, T., Y. Shibata, and T. Yamamoto, *A deep-etching study of the guinea pig tracheal cilium*
591 *with special reference to the ciliary transitional region.* J Ultrastruct Res, 1984. **89**(1): p. 34-41.
592 8. Reiter, J.F., O.E. Blacque, and M.R. Leroux, *The base of the cilium: roles for transition fibres*
593 *and the transition zone in ciliary formation, maintenance and compartmentalization.* EMBO Rep,
594 2012. **13**(7): p. 608-18.
595 9. Dean, S., et al., *Cilium transition zone proteome reveals compartmentalization and differential*
596 *dynamics of ciliopathy complexes.* Proc Natl Acad Sci U S A, 2016. **113**(35): p. E5135-43.
597 10. Gorden, N.T., et al., *CC2D2A is mutated in Joubert syndrome and interacts with the ciliopathy-*
598 *associated basal body protein CEP290.* Am J Hum Genet, 2008. **83**(5): p. 559-71.
599 11. Li, C., et al., *MKS5 and CEP290 Dependent Assembly Pathway of the Ciliary Transition Zone.*
600 PLoS Biol, 2016. **14**(3): p. e1002416.
601 12. Lambacher, N.J., et al., *TMEM107 recruits ciliopathy proteins to subdomains of the ciliary*
602 *transition zone and causes Joubert syndrome.* Nat Cell Biol, 2016. **18**(1): p. 122-31.
603 13. Avidor-Reiss, T. and M.R. Leroux, *Shared and Distinct Mechanisms of Compartmentalized and*
604 *Cytosolic Ciliogenesis.* Curr Biol, 2015. **25**(23): p. R1143-50.
605 14. Klena, N. and G. Pigino, *Structural Biology of Cilia and Intraflagellar Transport.* Annu Rev Cell
606 Dev Biol, 2022. **38**: p. 103-123.
607 15. Wei, Q., et al., *Transition fibre protein FBF1 is required for the ciliary entry of assembled*
608 *intraflagellar transport complexes.* Nat Commun, 2013. **4**: p. 2750.
609 16. Wang, L., et al., *Ciliary transition zone proteins coordinate ciliary protein composition and*
610 *ectosome shedding.* Nat Commun, 2022. **13**(1): p. 3997.
611 17. Reiter, J.F. and M.R. Leroux, *Genes and molecular pathways underpinning ciliopathies.* Nat
612 Rev Mol Cell Biol, 2017. **18**(9): p. 533-547.
613 18. Woolley, D., *The molecular motors of cilia and eukaryotic flagella.* Essays Biochem, 2000. **35**:
614 p. 103-15.
615 19. Leung, M.R., et al., *The multi-scale architecture of mammalian sperm flagella and implications*
616 *for ciliary motility.* EMBO J, 2021. **40**(7): p. e107410.
617 20. Miki, K., et al., *Targeted disruption of the Akap4 gene causes defects in sperm flagellum and*
618 *motility.* Dev Biol, 2002. **248**(2): p. 331-42.
619 21. Eddy, E.M., K. Toshimori, and D.A. O'Brien, *Fibrous sheath of mammalian spermatozoa.*
620 Microsc Res Tech, 2003. **61**(1): p. 103-15.
621 22. Brown, P.R., et al., *A-kinase anchoring protein 4 binding proteins in the fibrous sheath of the*
622 *sperm flagellum.* Biol Reprod, 2003. **68**(6): p. 2241-8.
623 23. Miyata, H., et al., *SPATA33 localizes calcineurin to the mitochondria and regulates sperm*
624 *motility in mice.* Proc Natl Acad Sci U S A, 2021. **118**(35).
625 24. Pleuger, C., et al., *Haploid male germ cells-the Grand Central Station of protein transport.* Hum
626 Reprod Update, 2020.
627 25. Gu, N.H., et al., *Comparative analysis of mammalian sperm ultrastructure reveals relationships*
628 *between sperm morphology, mitochondrial functions and motility.* Reprod Biol Endocrinol, 2019.
629 **17**(1): p. 66.
630 26. Ricci, M. and W.G. Breed, *Morphogenesis of the fibrous sheath in the marsupial spermatozoon.*
631 J Anat, 2005. **207**(2): p. 155-64.
632 27. Fawcett, D.W., *The mammalian spermatozoon.* Dev Biol, 1975. **44**(2): p. 394-436.
633 28. Kissel, H., et al., *The Sept4 septin locus is required for sperm terminal differentiation in mice.*
634 Dev Cell, 2005. **8**(3): p. 353-64.
635 29. Avidor-Reiss, T., A. Ha, and M.L. Basiri, *Transition Zone Migration: A Mechanism for*
636 *Cytoplasmic Ciliogenesis and Postaxonemal Centriole Elongation.* Cold Spring Harb Perspect
637 Biol, 2017. **9**(8).
638 30. Kwitny, S., A.V. Klaus, and G.R. Hunnicutt, *The annulus of the mouse sperm tail is required to*
639 *establish a membrane diffusion barrier that is engaged during the late steps of spermiogenesis.*
640 Biol Reprod, 2010. **82**(4): p. 669-78.
641 31. Kuo, Y.C., et al., *SEPT12 mutations cause male infertility with defective sperm annulus.* Hum
642 Mutat, 2012. **33**(4): p. 710-9.
643 32. Shen, Y.R., et al., *SEPT12 phosphorylation results in loss of the septin ring/sperm annulus,*
644 *defective sperm motility and poor male fertility.* PLoS Genet, 2017. **13**(3): p. e1006631.
645 33. Ho, H.C. and S. Wey, *Three dimensional rendering of the mitochondrial sheath morphogenesis*
646 *during mouse spermiogenesis.* Microsc Res Tech, 2007. **70**(8): p. 719-23.
647 34. Nagirnaja, L., et al., *Diverse monogenic subforms of human spermatogenic failure.* Nat
648 Commun, 2022. **13**(1): p. 7953.

- 649 35. Houston, B.J., et al., *A systematic review of the validated monogenic causes of human male*
650 *infertility: 2020 update and a discussion of emerging gene-disease relationships.* Hum Reprod
651 Update, 2021. **28**(1): p. 15-29.
- 652 36. Barbelanne, M., et al., *Opposing post-translational modifications regulate Cep76 function to*
653 *suppress centriole amplification.* Oncogene, 2016. **35**(41): p. 5377-5387.
- 654 37. Tsang, W.Y., et al., *Cep76, a centrosomal protein that specifically restrains centriole*
655 *reduplication.* Dev Cell, 2009. **16**(5): p. 649-60.
- 656 38. Fagerberg, L., et al., *Analysis of the human tissue-specific expression by genome-wide*
657 *integration of transcriptomics and antibody-based proteomics.* Mol Cell Proteomics, 2014. **13**(2):
658 p. 397-406.
- 659 39. Avidor-Reiss, T. and E.L. Fishman, *It Takes Two (Centrioles) to Tango.* Reproduction, 2018.
- 660 40. Zhang, D. and L. Aravind, *Novel transglutaminase-like peptidase and C2 domains elucidate the*
661 *structure, biogenesis and evolution of the ciliary compartment.* Cell Cycle, 2012. **11**(20): p.
662 3861-75.
- 663 41. Lindeboom, R.G., F. Supek, and B. Lehner, *The rules and impact of nonsense-mediated mRNA*
664 *decay in human cancers.* Nat Genet, 2016. **48**(10): p. 1112-8.
- 665 42. Yang, K., et al., *The small heat shock protein ODF1/HSPB10 is essential for tight linkage of*
666 *sperm head to tail and male fertility in mice.* Mol Cell Biol, 2012. **32**(1): p. 216-25.
- 667 43. Shang, Y., et al., *Essential role for SUN5 in anchoring sperm head to the tail.* Elife, 2017. **6**.
- 668 44. Hwang, J.Y., et al., *Genetic Defects in DNAH2 Underlie Male Infertility With Multiple*
669 *Morphological Abnormalities of the Sperm Flagella in Humans and Mice.* Front Cell Dev Biol,
670 2021. **9**: p. 662903.
- 671 45. Li, Y., et al., *DNAH2 is a novel candidate gene associated with multiple morphological*
672 *abnormalities of the sperm flagella.* Clin Genet, 2019. **95**(5): p. 590-600.
- 673 46. Lehti, M.S. and A. Sironen, *Formation and function of the manchette and flagellum during*
674 *spermatogenesis.* Reproduction, 2016. **151**(4): p. R43-54.
- 675 47. Larsson, M., et al., *The spatial and temporal expression of Tekt1, a mouse tektin C homologue,*
676 *during spermatogenesis suggest that it is involved in the development of the sperm tail basal*
677 *body and axoneme.* Eur J Cell Biol, 2000. **79**(10): p. 718-25.
- 678 48. Avasthi, P., et al., *Germline deletion of Cetn1 causes infertility in male mice.* J Cell Sci, 2013.
679 **126**(Pt 14): p. 3204-13.
- 680 49. Basiri, M.L., et al., *A migrating ciliary gate compartmentalizes the site of axoneme assembly in*
681 *Drosophila spermatids.* Curr Biol, 2014. **24**(22): p. 2622-31.
- 682 50. Guan, J., M. Kinoshita, and L. Yuan, *Spatiotemporal association of DNAJB13 with the annulus*
683 *during mouse sperm flagellum development.* BMC Dev Biol, 2009. **9**: p. 23.
- 684 51. Xu, K., et al., *Lack of AKAP3 disrupts integrity of the subcellular structure and proteome of*
685 *mouse sperm and causes male sterility.* Development, 2020. **147**(2).
- 686 52. Williams, C.L., et al., *MKS and NPHP modules cooperate to establish basal body/transition*
687 *zone membrane associations and ciliary gate function during ciliogenesis.* J Cell Biol, 2011.
688 **192**(6): p. 1023-41.
- 689 53. Garcia-Gonzalo, F.R. and J.F. Reiter, *Open Sesame: How Transition Fibers and the Transition*
690 *Zone Control Ciliary Composition.* Cold Spring Harb Perspect Biol, 2017. **9**(2).
- 691 54. Wu, Z., et al., *CEP290 is essential for the initiation of ciliary transition zone assembly.* PLoS
692 Biol, 2020. **18**(12): p. e3001034.
- 693 55. Rachel, R.A., et al., *CEP290 alleles in mice disrupt tissue-specific cilia biogenesis and*
694 *recapitulate features of syndromic ciliopathies.* Human Molecular Genetics, 2015. **24**(13): p.
695 3775-3791.
- 696 56. Eddy, E.M., et al., *Intermediate filament-like proteins in the fibrous sheath of the mouse sperm*
697 *flagellum.* Ann N Y Acad Sci, 1991. **637**: p. 224-39.
- 698 57. Mandal, A., et al., *FSP95, a testis-specific 95-kilodalton fibrous sheath antigen that undergoes*
699 *tyrosine phosphorylation in capacitated human spermatozoa.* Biol Reprod, 1999. **61**(5): p.
700 1184-97.
- 701 58. Otani, H., et al., *Development of mitochondrial helical sheath in the middle piece of the mouse*
702 *spermatid tail: regular dispositions and synchronized changes.* Anat Rec, 1988. **222**(1): p. 26-
703 33.
- 704 59. Ihara, M., et al., *Cortical organization by the septin cytoskeleton is essential for structural and*
705 *mechanical integrity of mammalian spermatozoa.* Dev Cell, 2005. **8**(3): p. 343-52.
- 706 60. Shimada, K., et al., *ARMC12 regulates spatiotemporal mitochondrial dynamics during*
707 *spermiogenesis and is required for male fertility.* Proc Natl Acad Sci U S A, 2021. **118**(6).

- 708 61. Ng, P.C. and S. Henikoff, *SIFT: Predicting amino acid changes that affect protein function*.
709 Nucleic Acids Res, 2003. **31**(13): p. 3812-4.
710 62. Adzhubei, I.A., et al., *A method and server for predicting damaging missense mutations*. Nat
711 Methods, 2010. **7**(4): p. 248-9.
712 63. Houston, B.J., et al., *The Sertoli cell expressed gene secernin-1 (Scrn1) is dispensable for male*
713 *fertility in the mouse*. Dev Dyn, 2021. **250**(7): p. 922-931.
714 64. Houston, B.J., D.F. Conrad, and M.K. O'Bryan, *A framework for high-resolution phenotyping of*
715 *candidate male infertility mutants: from human to mouse*. Hum Genet, 2021. **140**(1): p. 155-
716 182.
717 65. Dunleavy, J.E.M., et al., *KATNB1 is a master regulator of multiple katanin enzymes in male*
718 *meiosis and haploid germ cell development*. Development, 2021. **148**(24).
719 66. Gibbs, G.M., et al., *Cysteine-rich secretory protein 4 is an inhibitor of transient receptor potential*
720 *M8 with a role in establishing sperm function*. Proc Natl Acad Sci U S A, 2011. **108**(17): p. 7034-
721 9.
722 67. Skinner, B.M., et al., *A high-throughput method for unbiased quantitation and categorization of*
723 *nuclear morphologydagger*. Biol Reprod, 2019. **100**(5): p. 1250-1260.
724 68. Dunleavy, J.E.M., et al., *Katanin-like 2 (KATNAL2) functions in multiple aspects of haploid male*
725 *germ cell development in the mouse*. PLoS Genet, 2017. **13**(11): p. e1007078.
726 69. Korneev, D., et al., *New Insights Into Sperm Ultrastructure Through Enhanced Scanning*
727 *Electron Microscopy*. Front Cell Dev Biol, 2021. **9**: p. 672592.
728 70. Netherton, J., et al., *Mass Spectrometry Reveals New Insights into the Production of*
729 *Superoxide Anions and 4-Hydroxyneononal Adducted Proteins in Human Sperm*. Proteomics,
730 2020. **20**(3-4): p. e2070024.
731 71. Dunleavy, J.E.M., A.E. O'Connor, and M.K. O'Bryan, *An optimised STAPUT method for the*
732 *purification of mouse spermatocyte and spermatid populations*. Mol Hum Reprod, 2019.

733
734

735 **Figure legends**

736 **Figure 1. CEP76 is essential for male fertility.** Wild type versus *Cep76* knockout data for A. Litter
737 size. B. Body weight. C. Testis weight. D. Epididymis weight. E. Daily sperm production per testis. F.
738 Epididymal sperm content. **** $p < 0.0001$. G, I. Histology of wild type and H, J. *Cep76* knockout testis
739 sections of stage VIII and stage IX tubules, respectively. Arrows in J point to retained spermatids as
740 evidence of spermiation failure. Sg = spermatogonia, Sc = spermatocyte, RS = round spermatid, ES =
741 elongating spermatid, S/C = Sertoli cell. K, L. Cauda epididymis sections are shown for wild type and
742 *Cep76* knockout. Scale bars are noted to equal 50 or 20 μm .

743

744 **Figure 2. CEP76 is required for normal sperm morphology, motility and tail length.** Wild type
745 versus *Cep76* knockout data for A. Total and B. Progressive sperm motility as assessed by computer
746 assisted sperm analysis. C. Sperm morphology – arrows denote abnormally shaped sperm heads. D.
747 Total sperm tail length. E. Sperm midpiece length as measured via MitoTracker staining. F. Sperm
748 annulus staining (SEPT4). Scale bar = 5 μm . G. Sperm annulus migration distance. H. Incidence of
749 SEPT4 staining in sperm. I. Incidence of sperm SUN5 staining. ** $p < 0.01$, **** $p < 0.0001$.

750

751 **Figure 3. CEP76 is required for accessory structure assembly and normal axoneme**
752 **ultrastructure.** Wild type sperm are shown in panels A, D, G and J; sperm from *Cep76* knockouts are
753 shown in panels B, C, E, F, H, I, K and L. **Top row** (A, B, C) – sperm midpiece cross-sections highlighted
754 a broadly normal axoneme in both genotypes, with evidence of mitochondrial and membrane
755 aggregation in knockout sperm. **Second row** (D, E, F) – sperm principal piece cross-sections
756 highlighted the absence of some microtubule doublets and outer dense fibres (arrow, E), and the
757 displacement of some microtubule doublets (black and white arrows, F) in knockout cells. **Third row**
758 (G, H, I) – midpiece longitudinal sections highlighted abnormal mitochondrial morphology (arrows, H)
759 and aggregation (arrow, I) in knockout cells. **Bottom row** (J, K, L) – longitudinal sections of the
760 midpiece-principal piece boundary revealed abnormal annulus formation (arrows point to predicted
761 annulus structures, K, L) and the consequential mixing of mitochondria and fibrous sheath structures in
762 knockout cells (K). MP = midpiece, PP = principal piece, An = annulus, FS = fibrous sheath, Mito =
763 mitochondria. Scale bars = 200 nm.

764

765 **Figure 4. Annulus, mitochondrial sheath and fibrous sheath formation are impaired in the**
766 **absence of CEP76.** Scanning electron microscopy on membrane stripped sperm revealed defects in
767 accessory structures in knockout sperm (B, C). MP = midpiece, An = annulus, FS = fibrous sheath.
768 Sperm nuclei are overlayed in purple, mitochondria in red, annuli in yellow and fibrous sheaths in blue.
769 High power images of the midpiece-principal piece boundary (D, E, F) revealed an abnormal annulus
770 region in knockout sperm and the core axoneme being exposed (arrows). Wild type mitochondria were
771 helically arranged with morphology normal (G), whereas mitochondria were poorly arranged (H) or
772 aggregated (I) in knockout cells. Fibrous sheath deposition was highly abnormal in the absence of
773 CEP76 (C, K, L) and appeared to be unanchored in knockout cells. Additionally, the slits present in wild
774 type sperm (J, arrows) were missing from knockout cells. Scale bars = 1 μ m. These defects were
775 quantified (M-P). M. Annulus normality assessment. N. Prevalence of exposed outer dense fibres
776 (ODFs). O. Mitochondrial sheath normality assessment (5 = best, 1 = worst). P. Fibrous sheath
777 normality assessment (3 = best, 1 = worst). *** $p < 0.001$, **** $p < 0.0001$.

778

779 **Figure 5. CEP76 is required for the loading of essential motility and fibrous sheath proteins into**
780 **the sperm tail.** Wild type versus *Cep76* knockout data for A. DNAH2 localisation in cauda epididymal

781 sperm. B. AKAP4 localisation in cauda epididymal sperm. Scale bars = 20 μ m. Arrows point to
782 accumulation of DNAH2 or AKAP4 in the neck region of sperm. The number of sperm with this neck
783 localisation was quantified, as shown in C and D for DNAH2 and AKAP4, respectively. The average tail
784 pixel intensity (per area) of DNAH2 and AKAP4 were quantified and are shown in E and F. *** $p <$
785 0.001, * $p < 0.05$.

786

787 **Table 1A. Proteins with significantly altered content in sperm from Cep76 knockouts.** Green
788 proteins are upregulated in sperm from knockout mice, blue proteins are downregulated.

789

790 **Table 1B. Proteins with significantly altered content in sperm from Cep76 knockouts, after**
791 **normalisation to alpha tubulin content.** All proteins were upregulated in sperm from knockout. Known
792 sperm tail proteins are highlighted orange. Other proteins are present throughout the entire sperm cell
793 or localisation is unknown.

794

795 **Supplementary Figure 1. CEP76 human genetic variant and Cep76 knockout mouse model.** A.
796 CEP76 mutation identified in an infertile man, including genetic coordinates and protein position. B.
797 CEP76 protein species alignment, including conserved amino acid (G, bolded + underlined), and total
798 protein identity across species. Red letters denote amino acids not conserved in zebrafish (*Danio rerio*)
799 and the affected amino acid in the infertile man. C. MetaDome assessment of the affected amino acid
800 and its tolerant to change, which was assessed as intolerant. D. The genetic variant affected exon 5 of
801 the human CEP76 protein, within the C2 (ciliary targeting, exons 4-6) domain. CEP76 additionally holds
802 a TGL (transglutaminase, exons 7-9) domain. E. Mouse full length *Cep76* transcript and *Cep76*
803 knockout transcript shown below (* denotes premature stop codon in exon 4). Red arrows denote where
804 guide RNAs for exon 3 removal targeted – intronic regions surrounding exon 3; orange arrows denote
805 approximate target sites of qPCR primers. F. *Cep76* expression as measured by qPCR in wild type and
806 knockout testes, relative to housekeeper *Ppia* expression. ** = $p < 0.01$.

807

808 **Supplementary Figure 2. Cep76 is a spermatid enriched gene.** A. *Cep76* expression across major
809 organs in mice as assessed by quantitative PCR (qPCR) relative to housekeeper *Ppia*. B. *Cep76*
810 expression in mouse testes during the first wave of spermatogenesis, relative to *Ppia*. Ages correspond

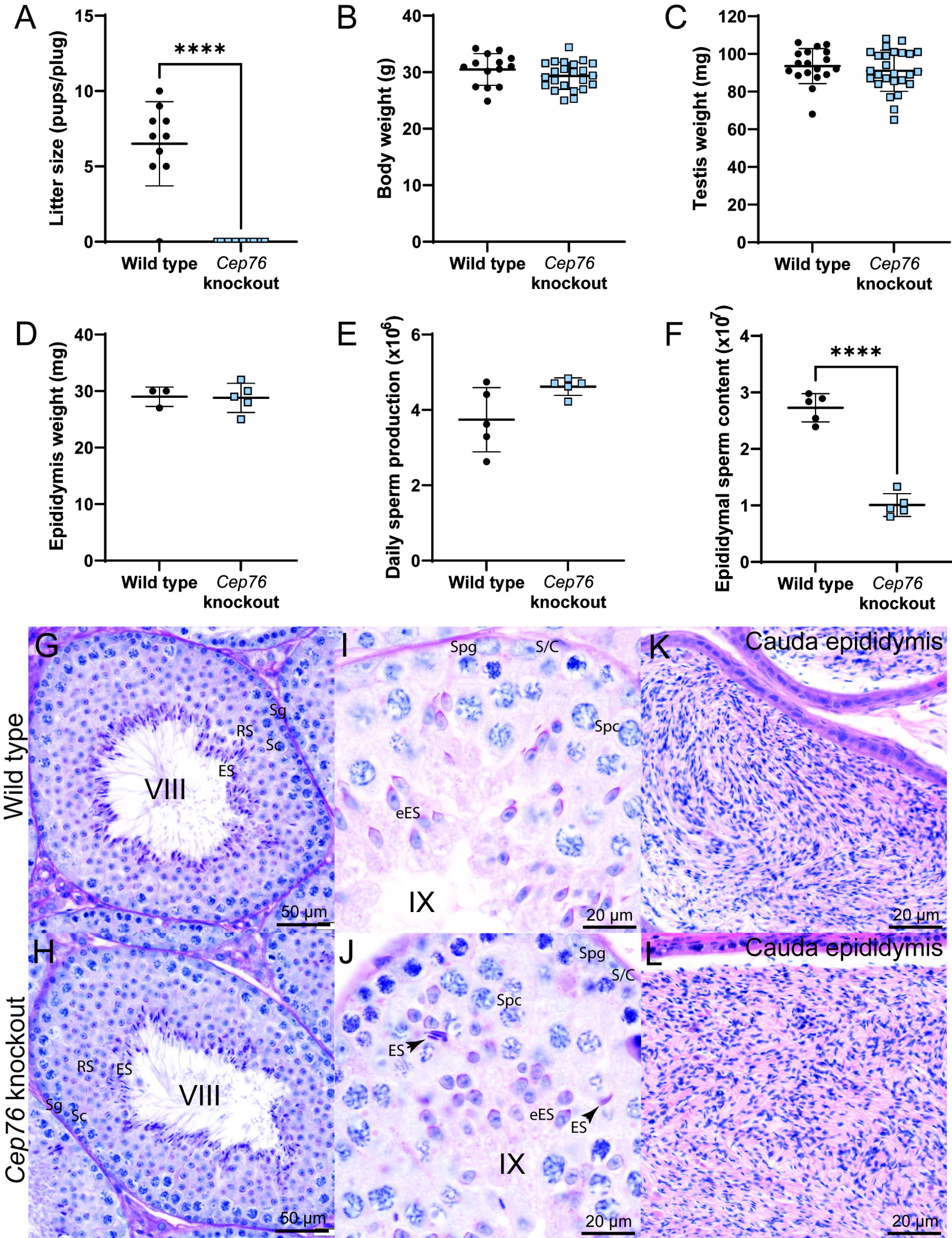
811 to the first appearance of different male germ cell types. C. *Cep76* expression in mouse testis cell types
812 as defined by single cell sequencing. Spg. = spermatogonia, P spc. = pachytene spermatocyte, sptd. =
813 spermatid.

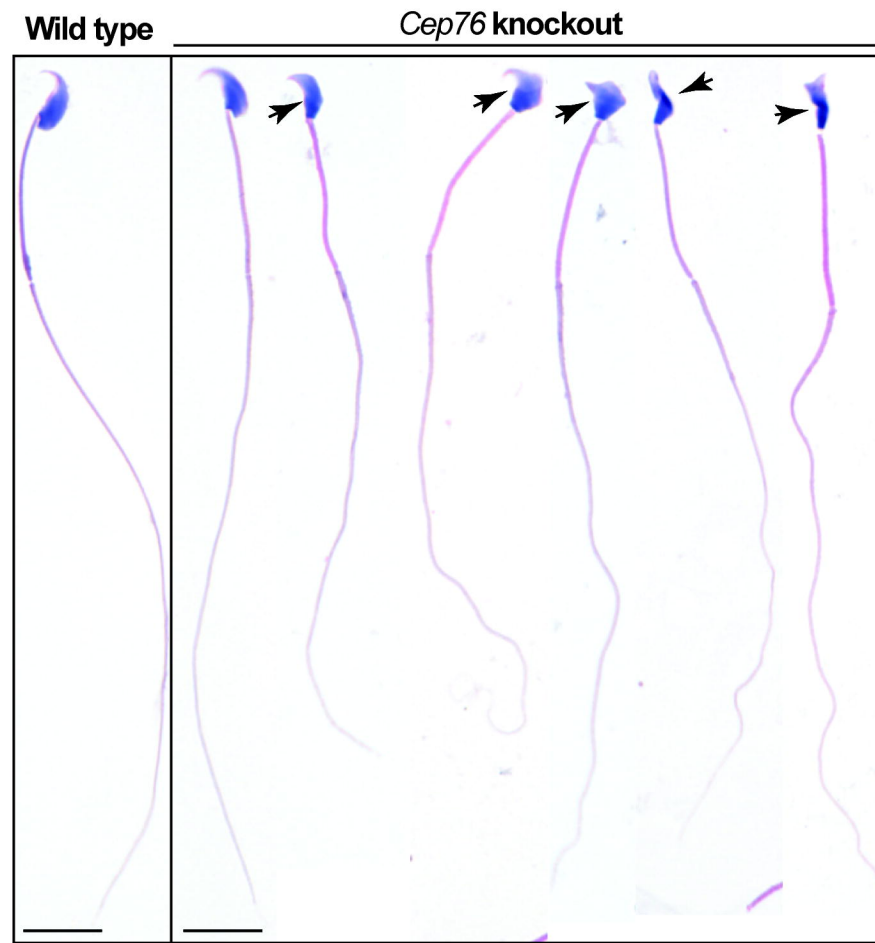
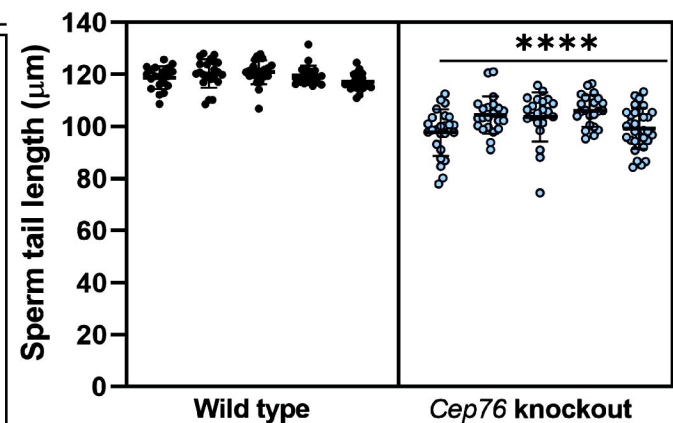
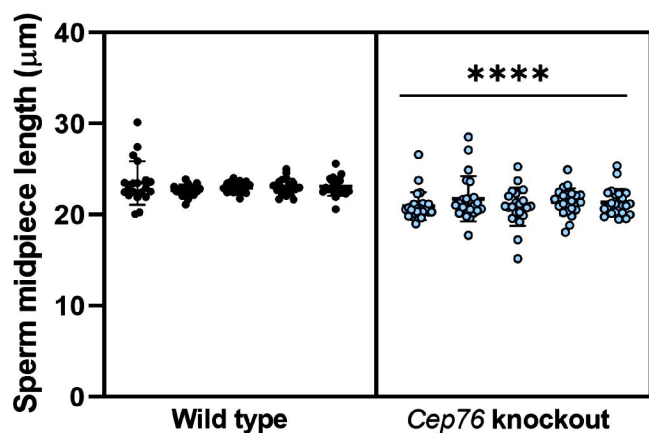
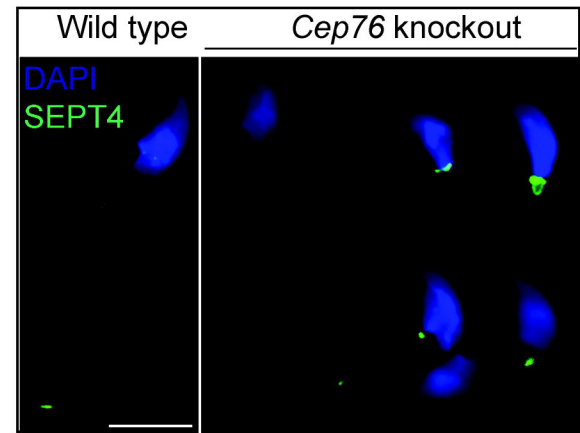
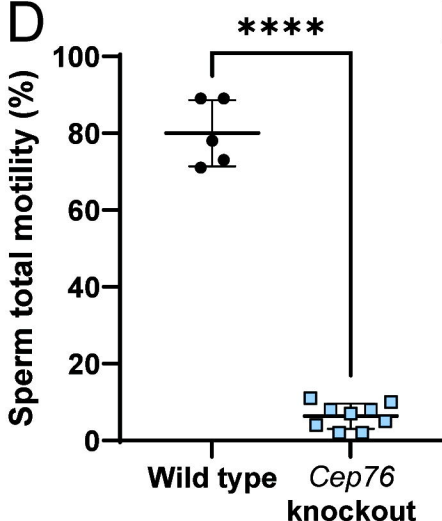
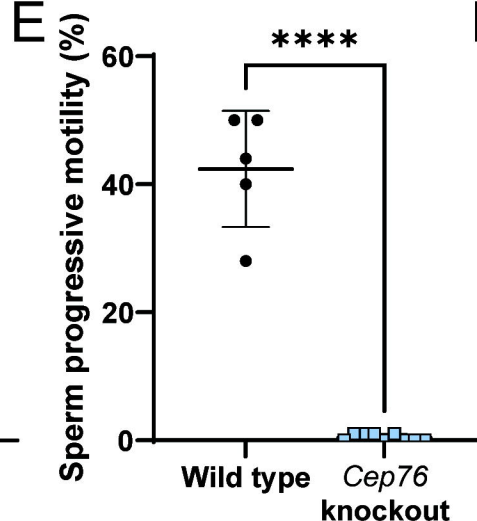
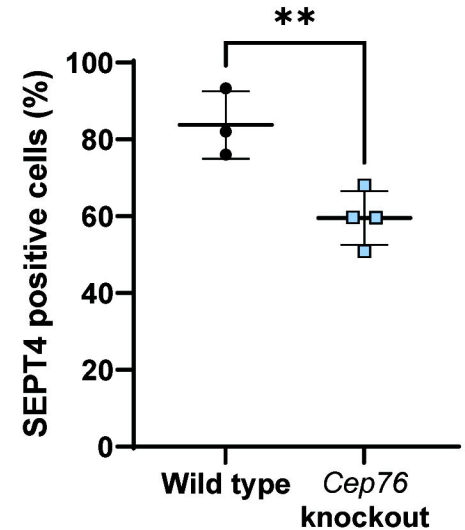
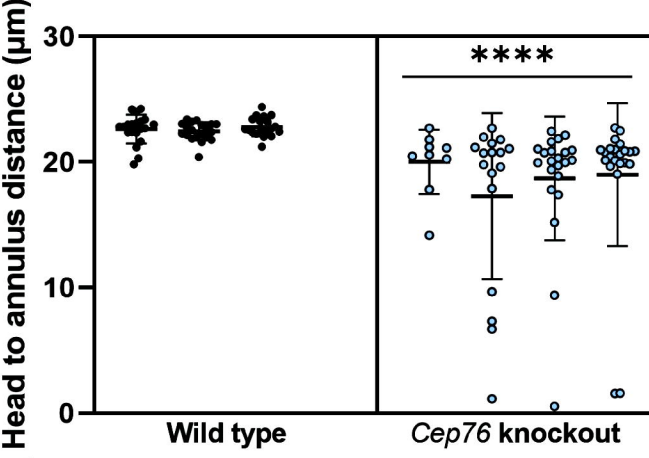
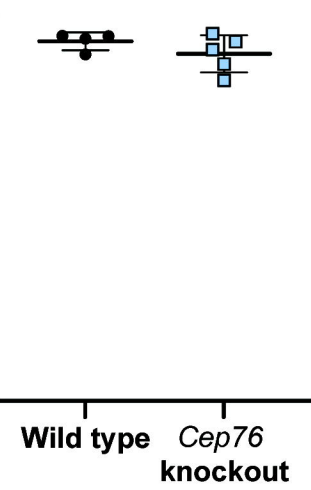
814

815 **Supplementary Figure 3. CEP76 is required for sperm head and acrosome shape but not normal**
816 **manchette formation.** A. Abnormal sperm head shape assessment. B. Abnormal sperm acrosome
817 formation assessment. C. Sperm decapitation assessment. D. Sperm head and acrosome morphology
818 assessment on cells stained with DAPI and PNA. E. Objective sperm head shape analysis and the
819 proportion of sperm falling into each Cluster. Cluster 1 are most normal through to Cluster 5 as the most
820 abnormal head shapes. Representative traces are shown for head shapes below each cluster. F.
821 Spermatids at stage IX, XI and II-III stained with alpha-tubulin to mark the manchette are shown. Scale
822 bars are 10 μ m in length. ** $p < 0.01$, **** $p < 0.0001$.

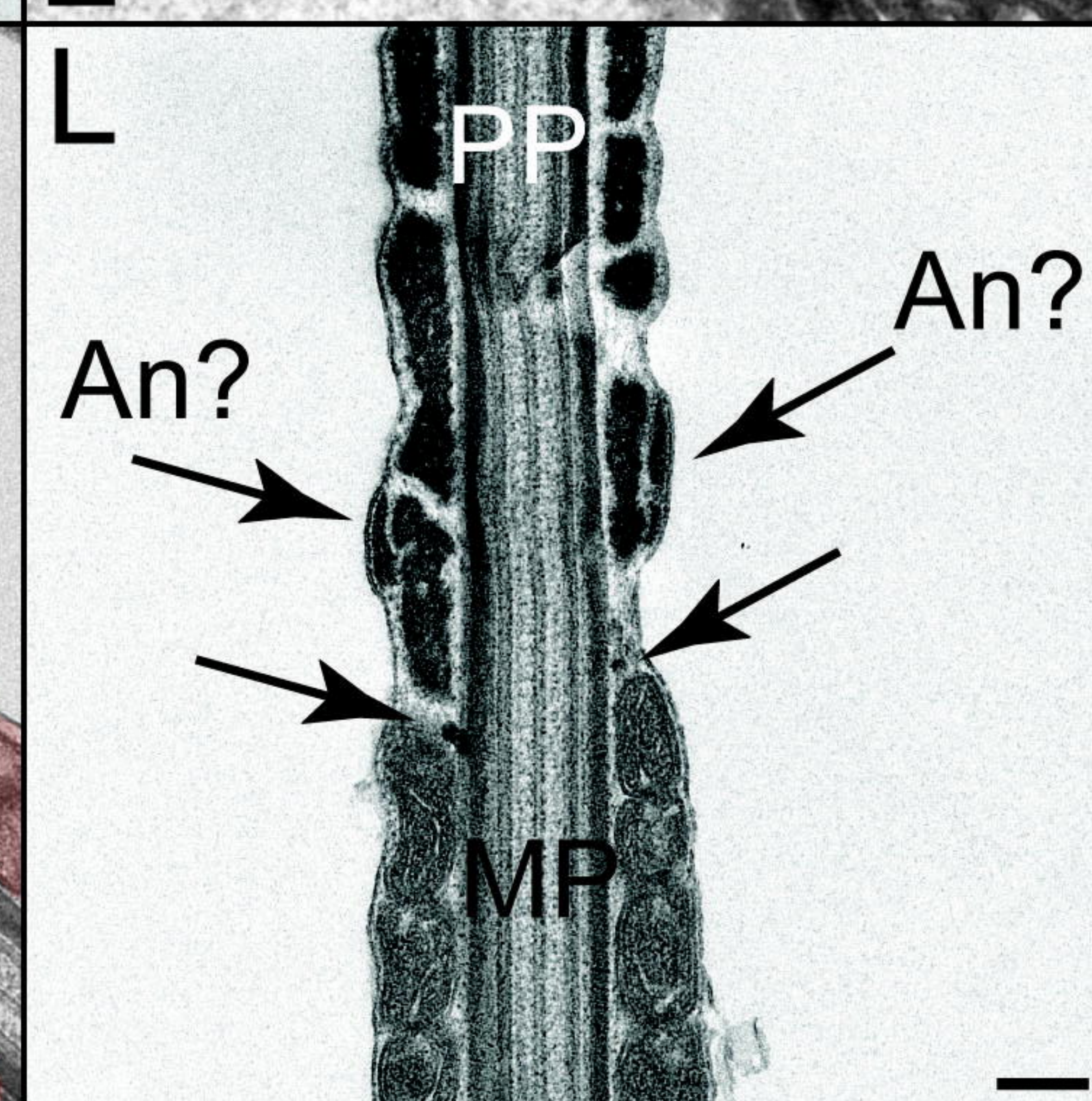
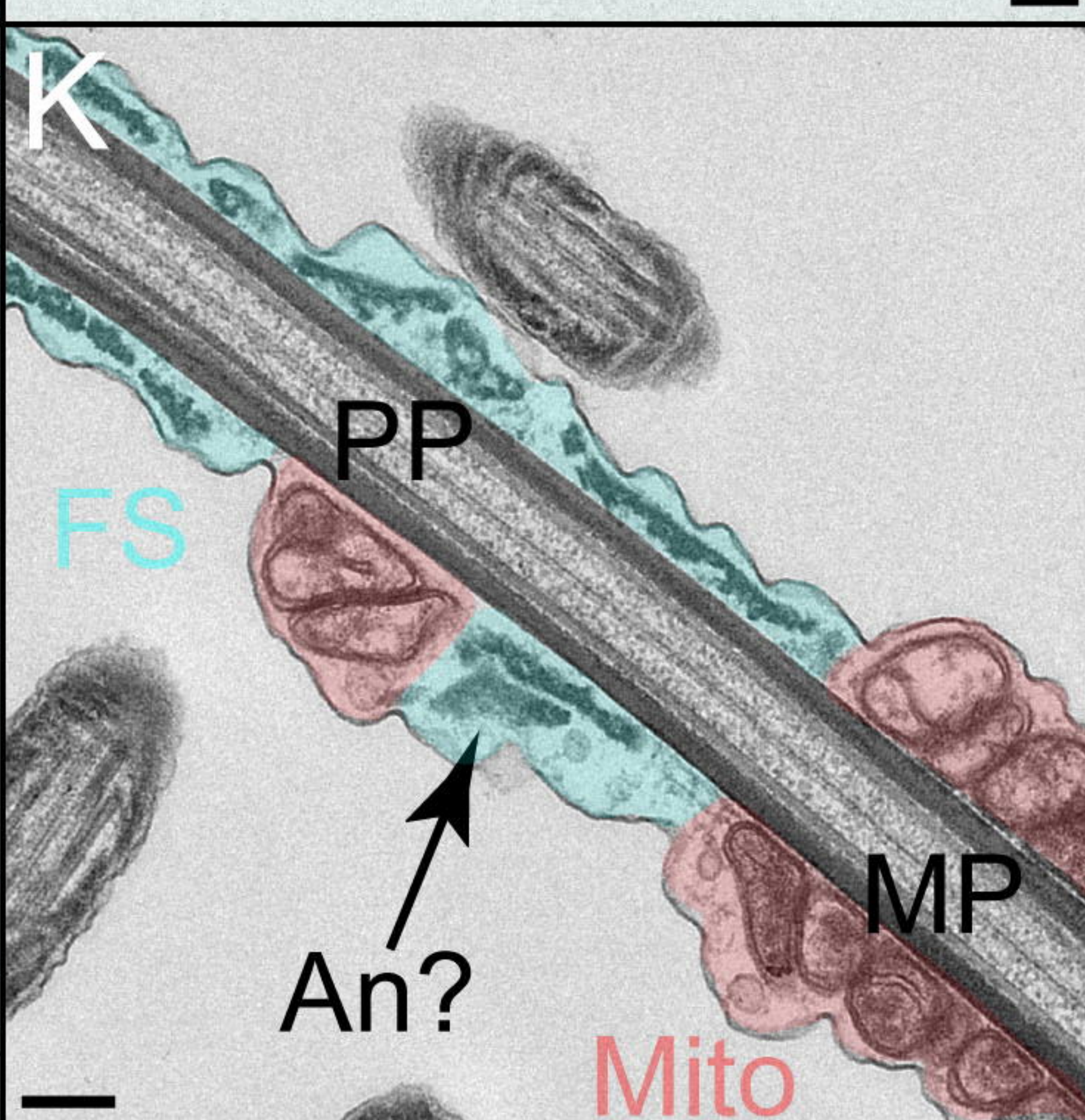
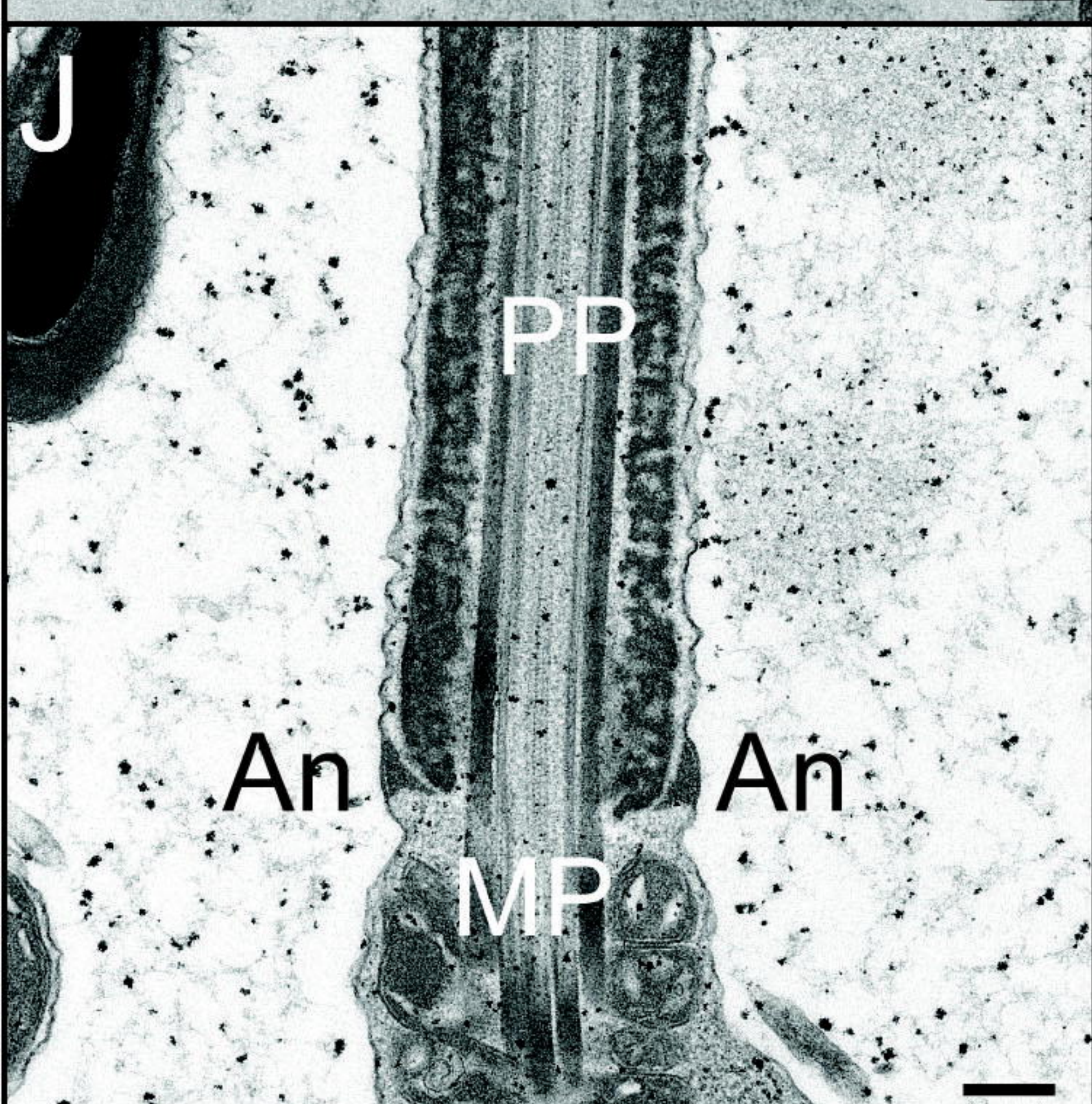
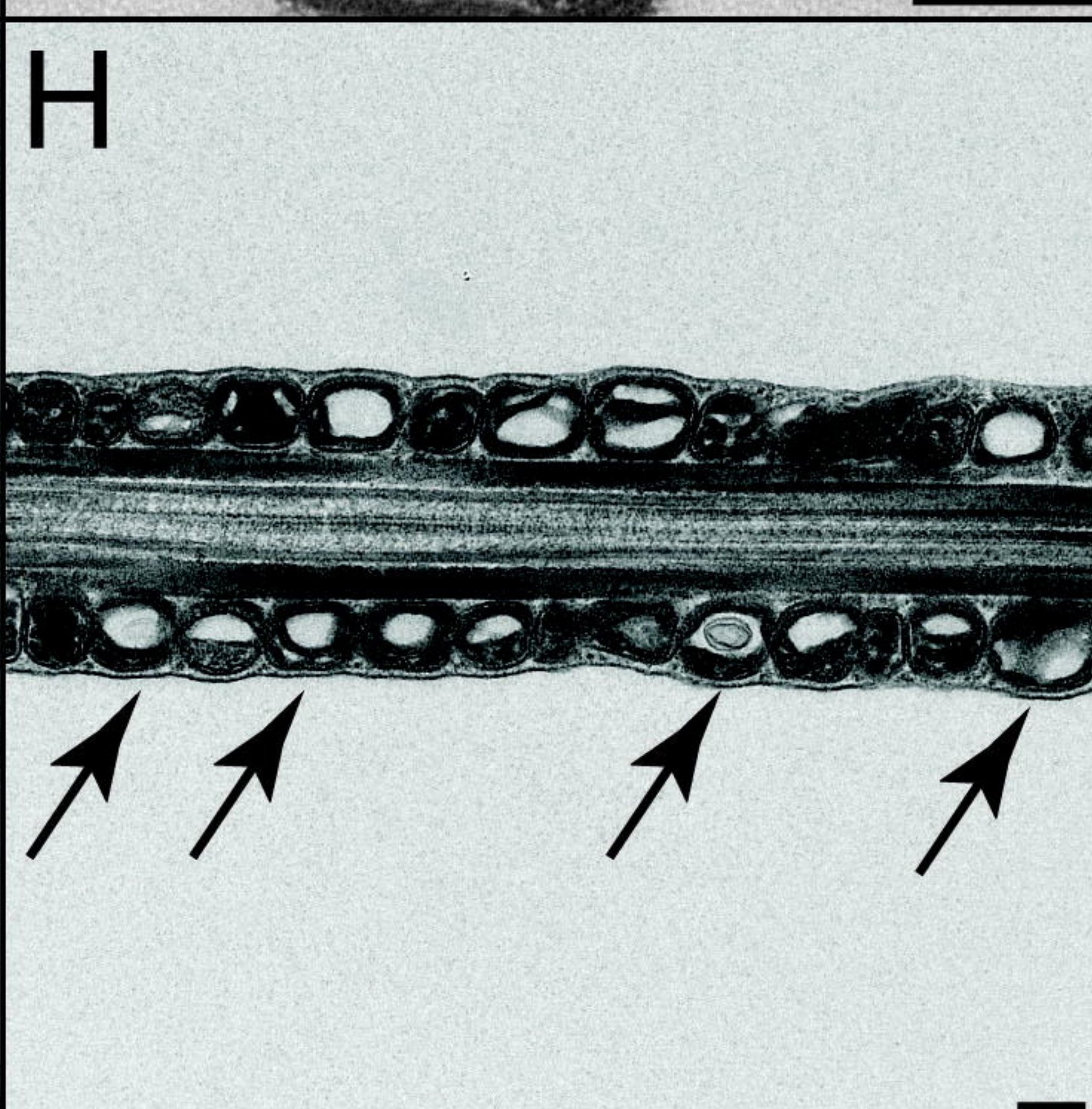
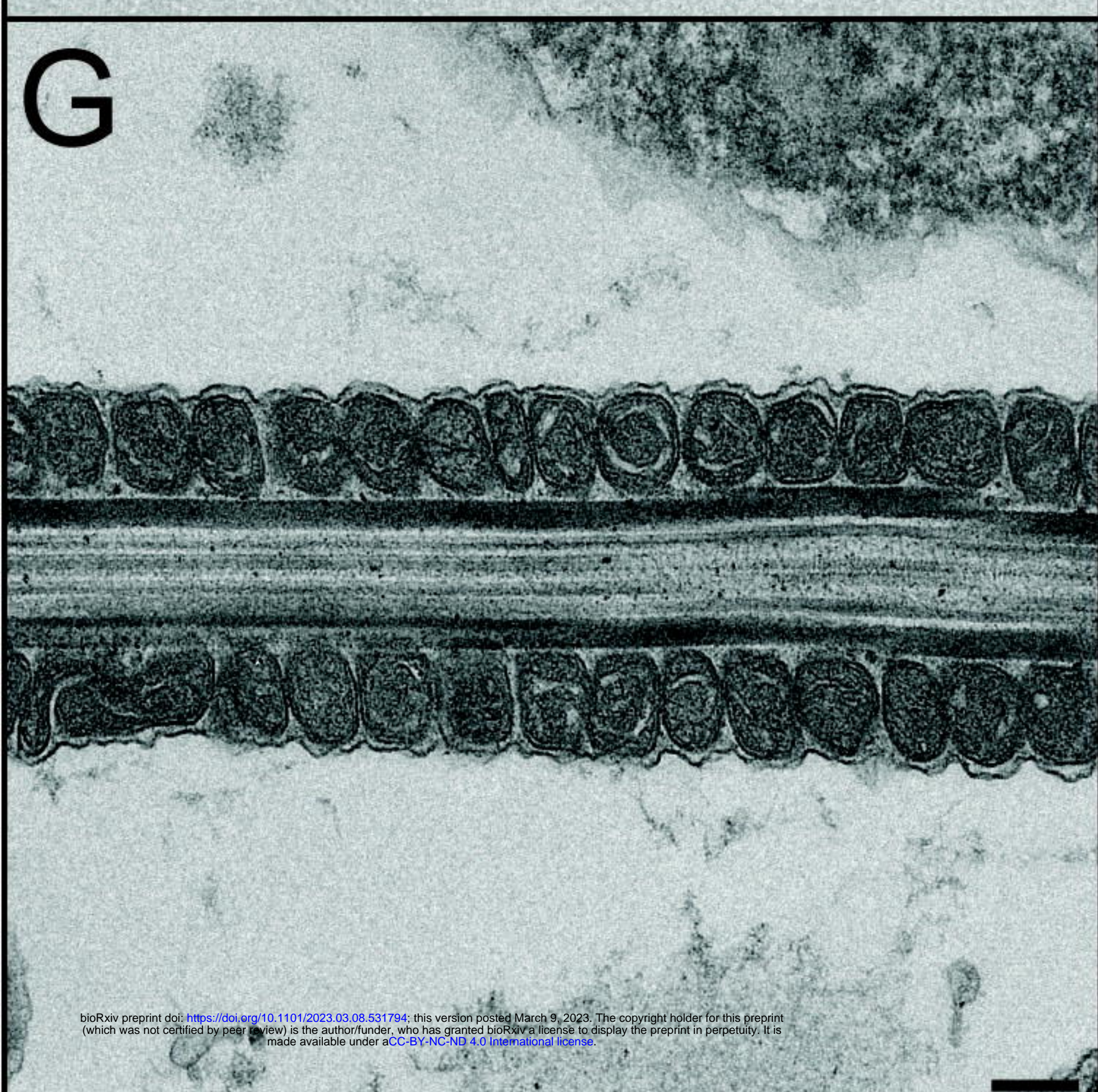
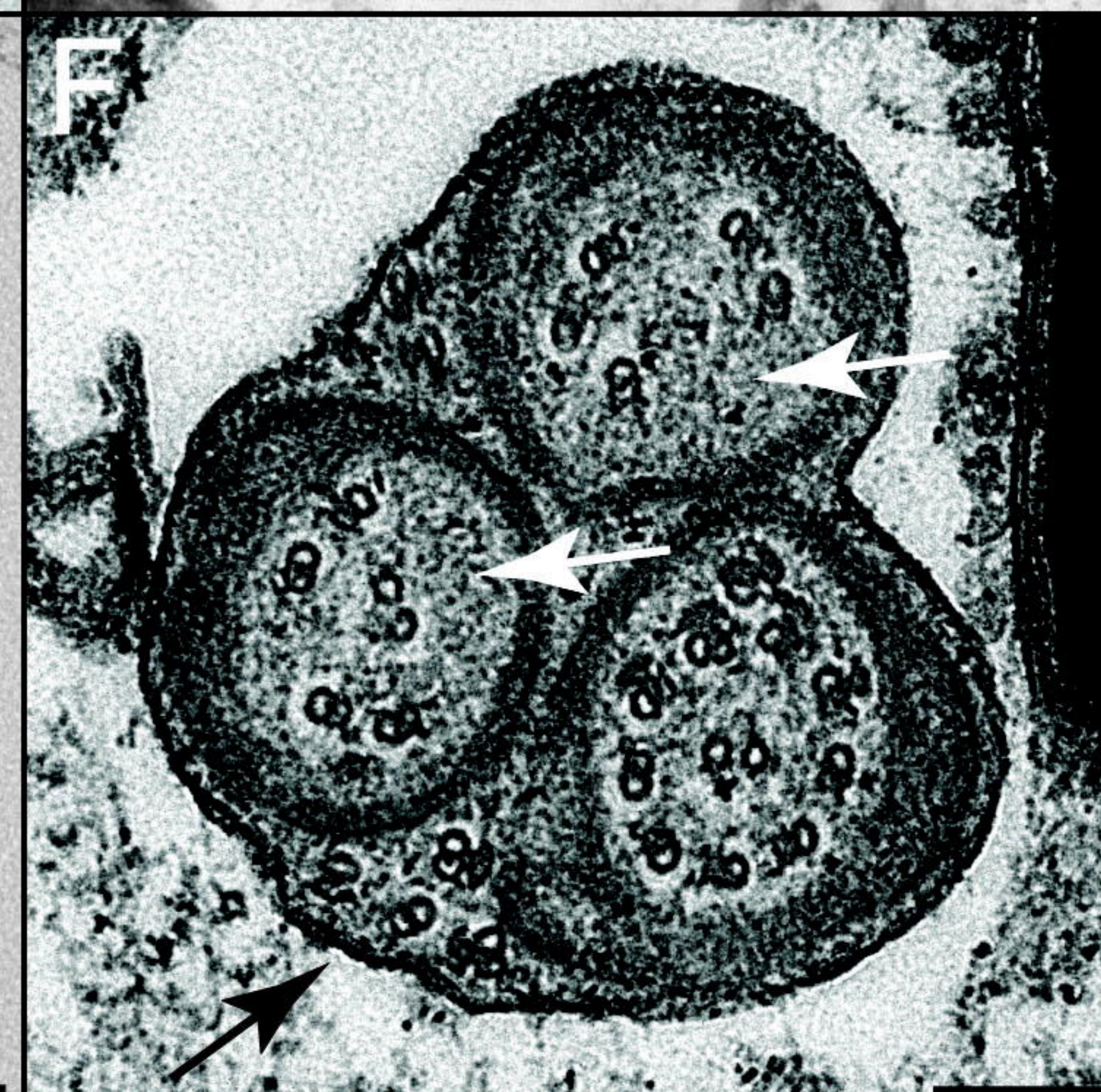
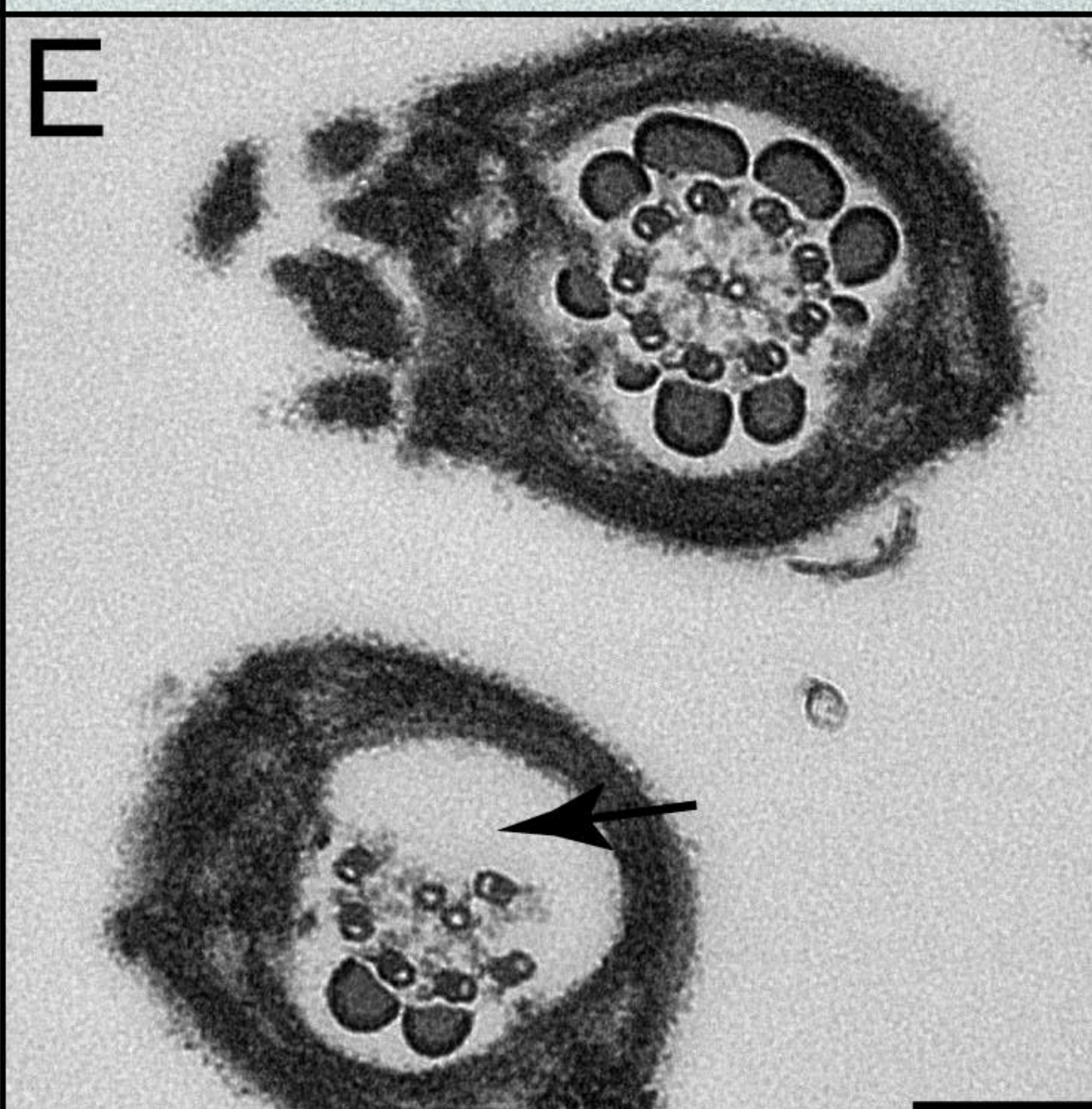
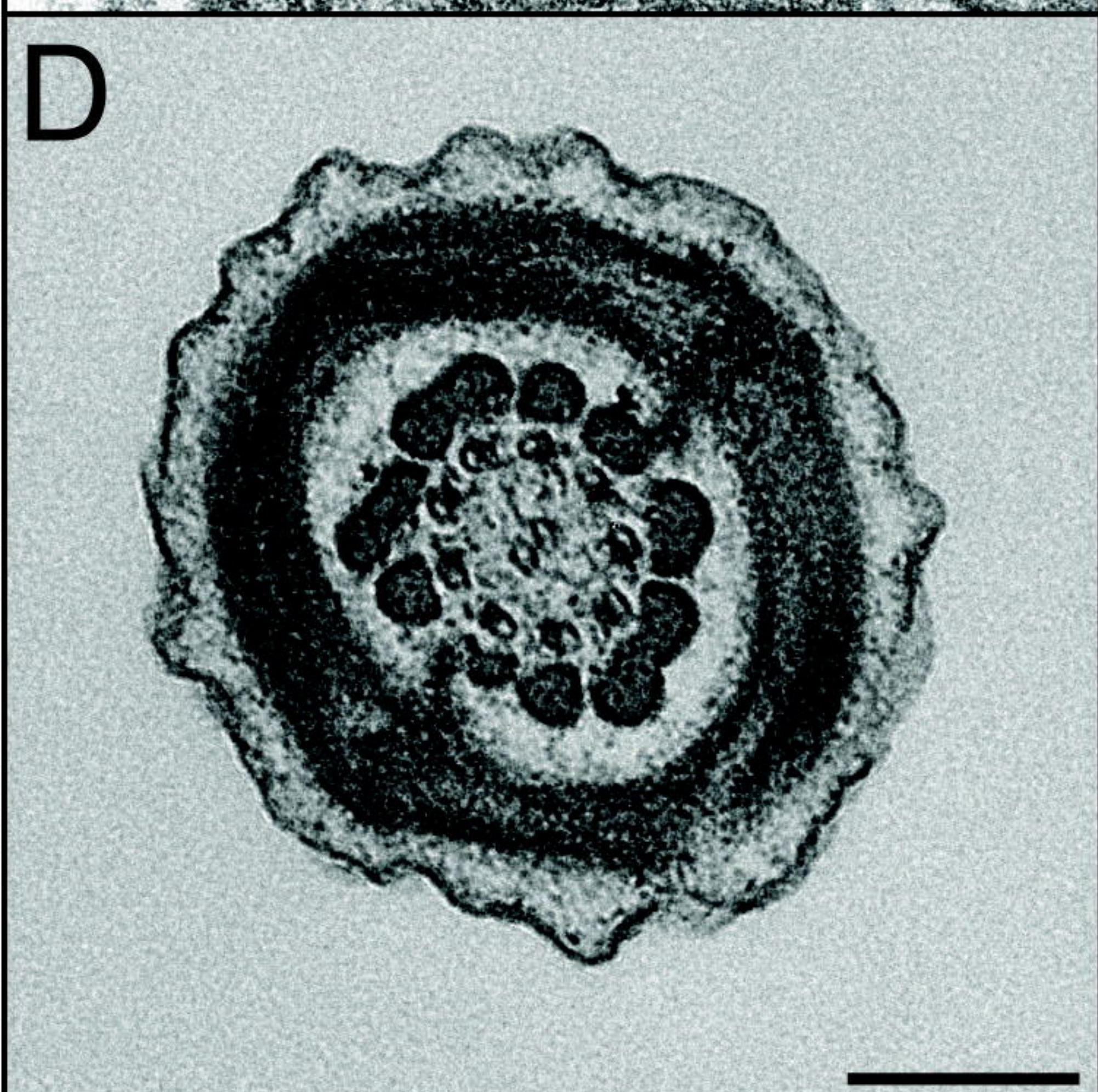
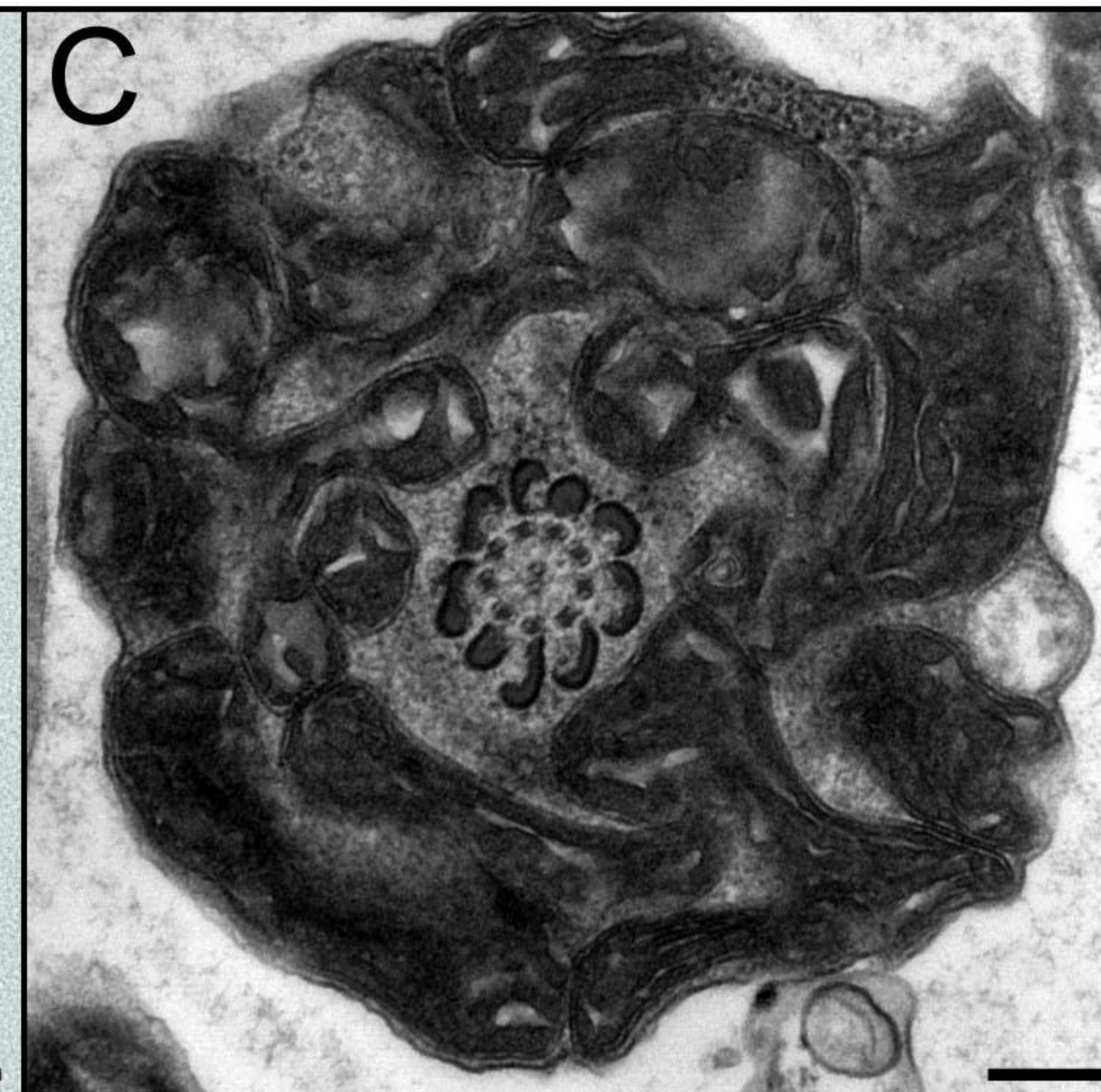
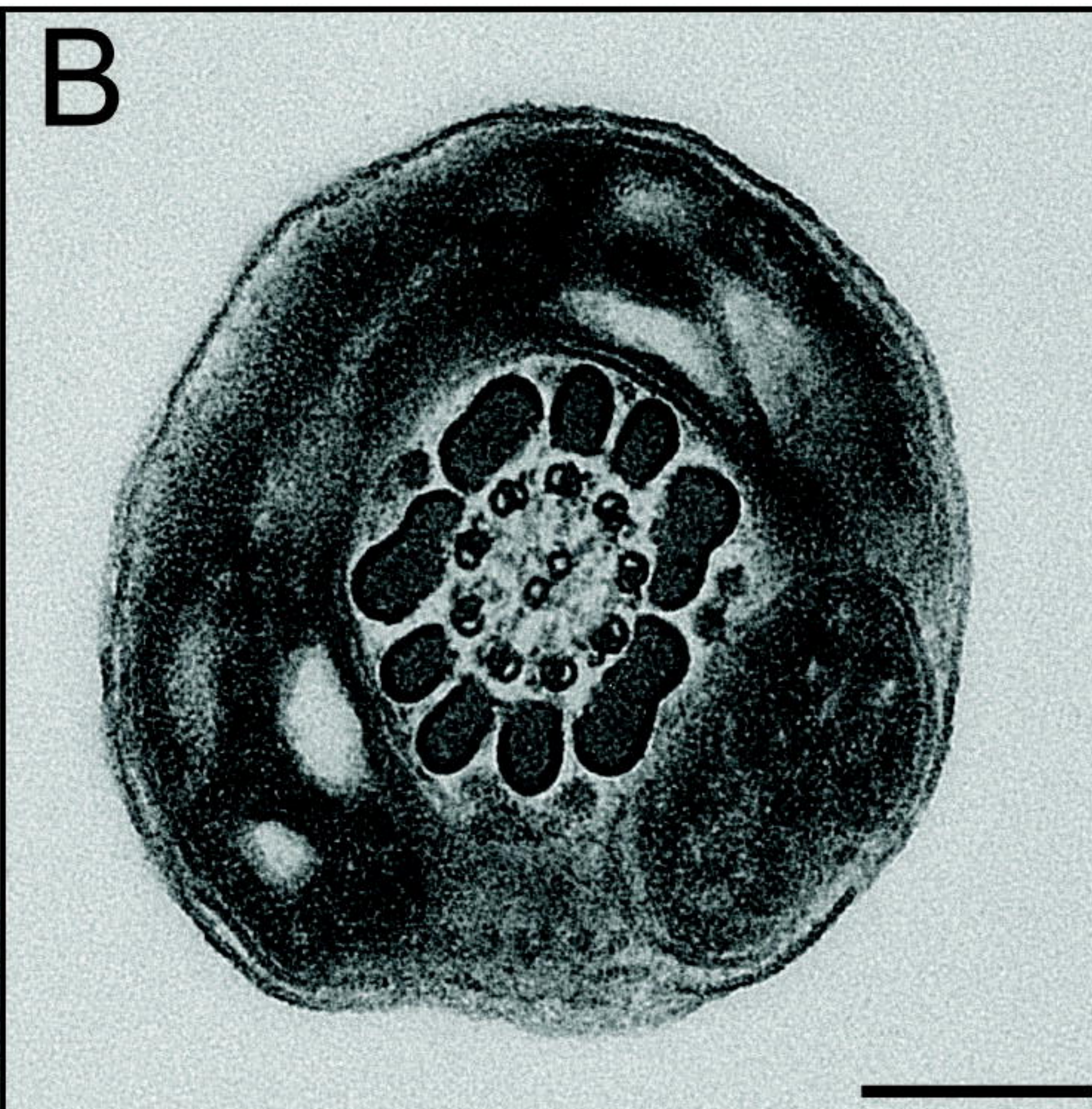
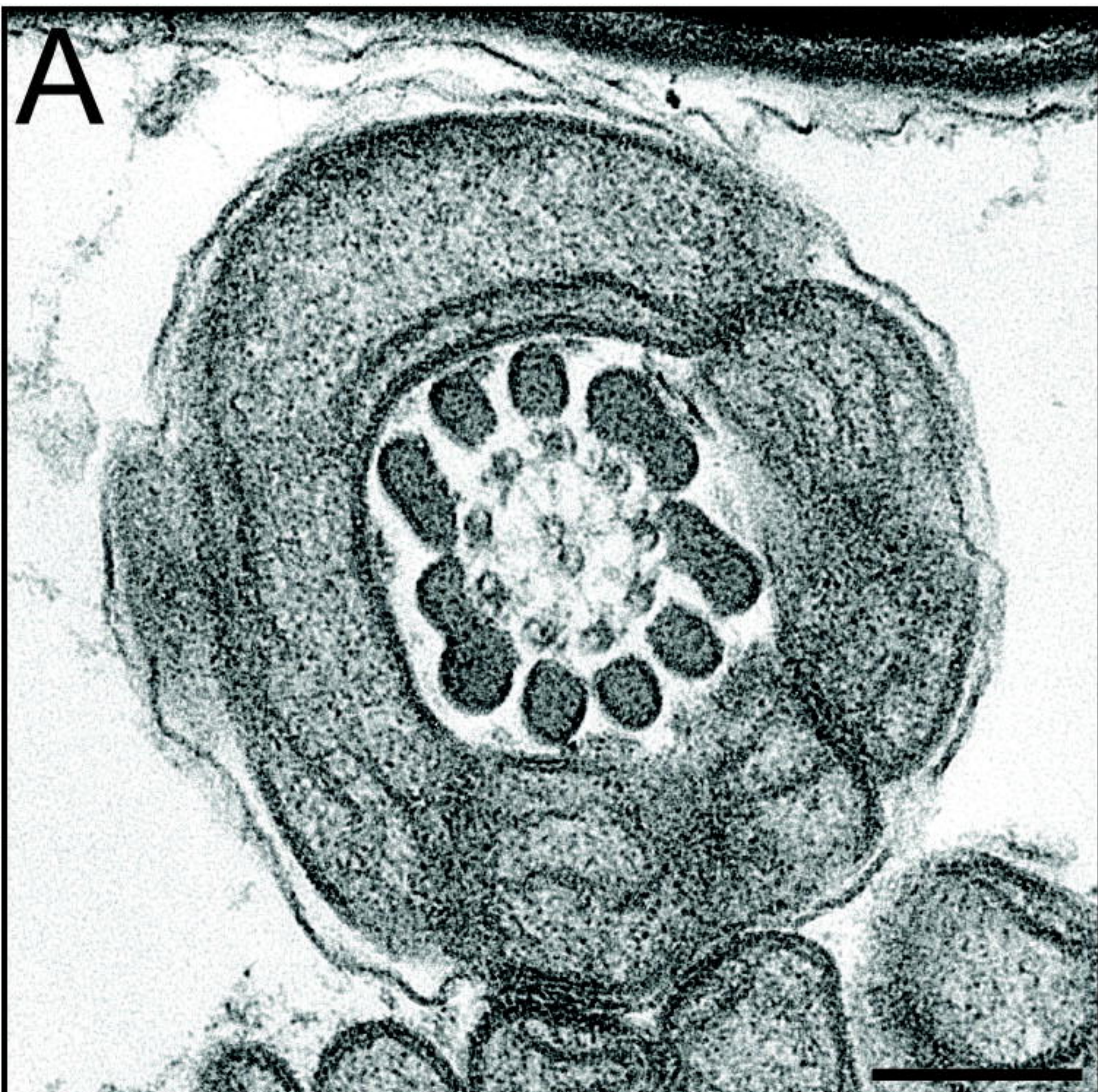
823

824 **Supplementary Figure 4. CEP76 is required for sperm neck integrity and suppression of**
825 **centriole duplication in male germ cells.** A-C. Scanning electron microscopy images of sperm heads
826 from wild type and *Cep76* knockout sperm. D-F. Transmission electron microscopy images of sperm
827 neck regions. Arrows and expanded dashed box denote potential granulated bodies (GB) throughout
828 the neck region in panel E. In panel F, the red arrows point to abnormal membrane folding. G, H.
829 Centriole number/content as defined by centrin staining. Arrows point to individual centriole components.
830 Scale bars = 2 μ m in all panels, except length in D-F where they are 1 μ m. I. Quantification of centriole
831 number in round and elongating spermatids, categories as 0, 2 or 3+. * $p < 0.05$, ** $p < 0.01$, ns = not
832 significant.

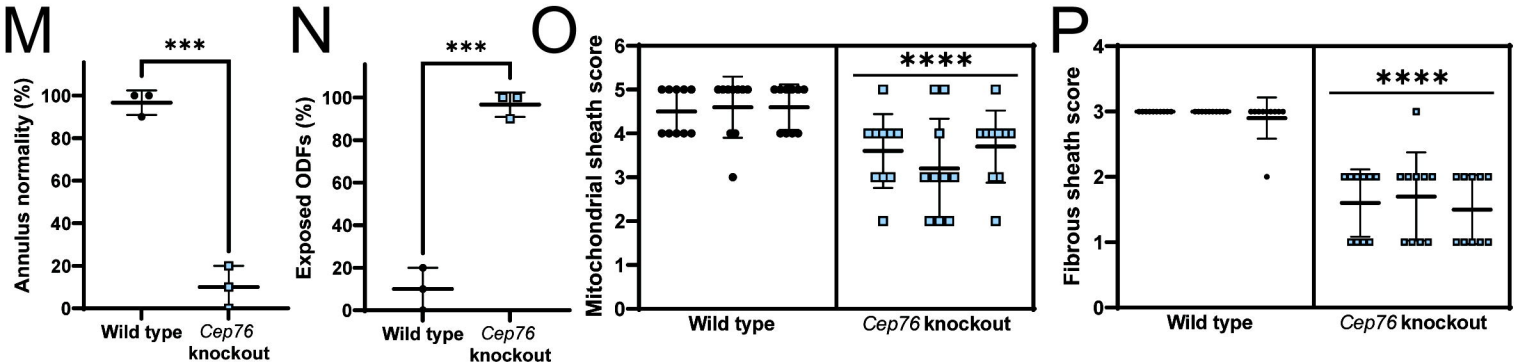
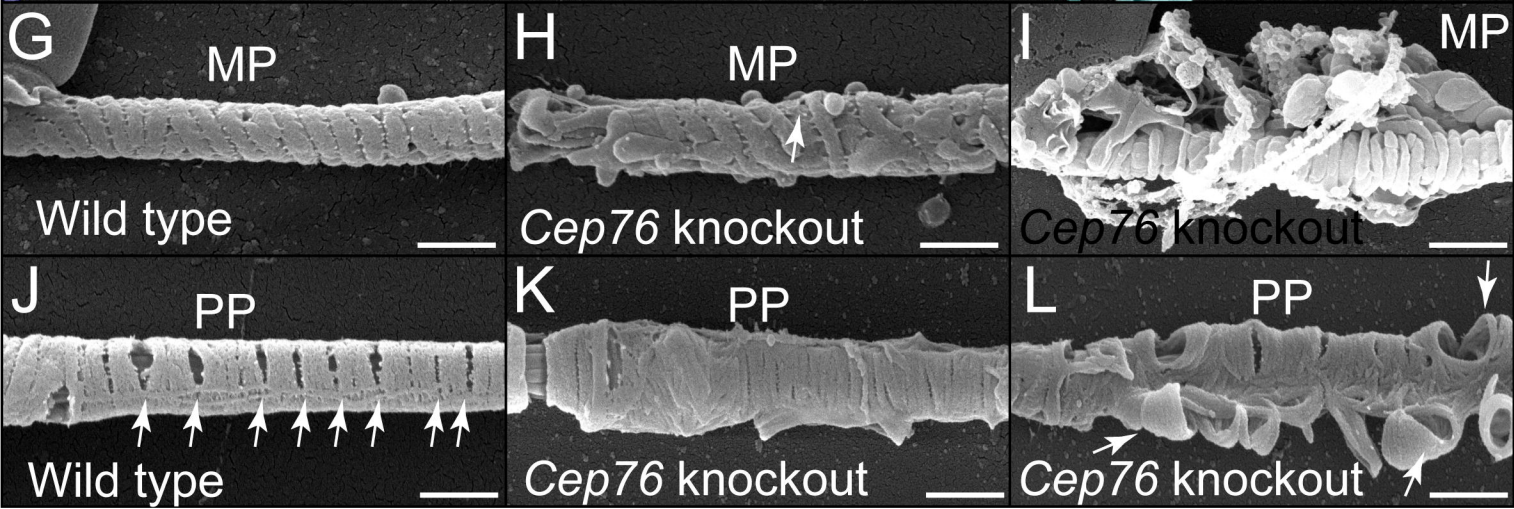
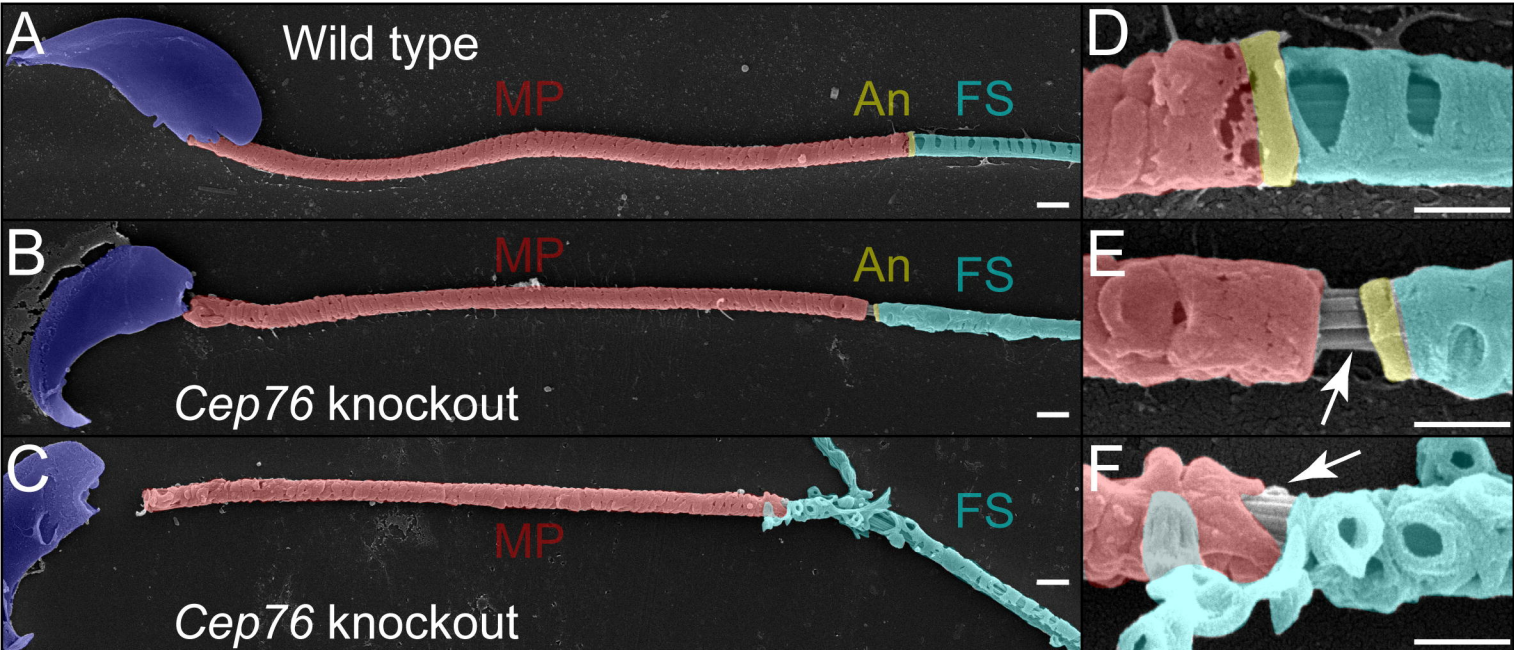


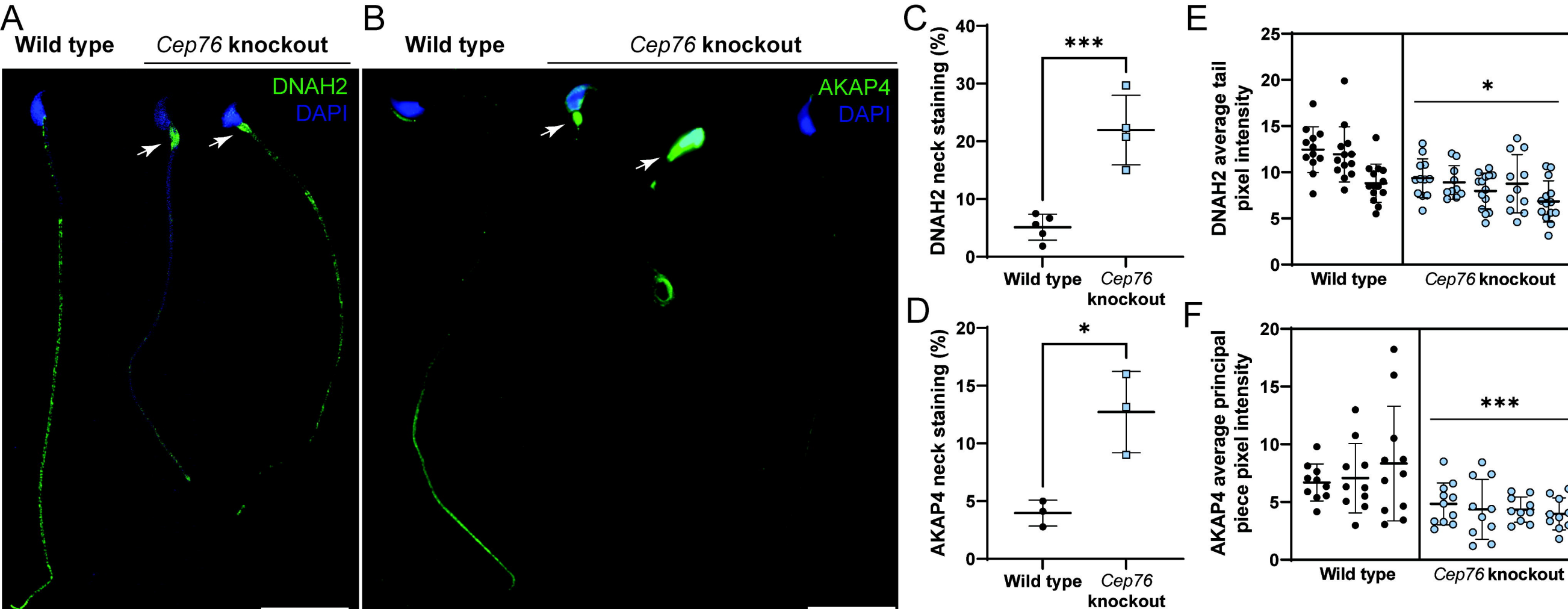
A**B****C****F****D****E****H****G****SUN5 positive sperm (%)**

Wild type



Cep76 knockout



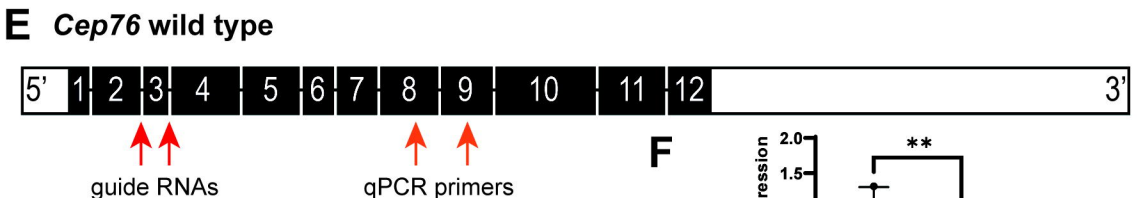
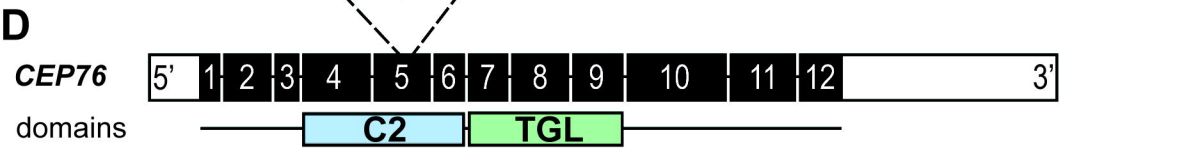
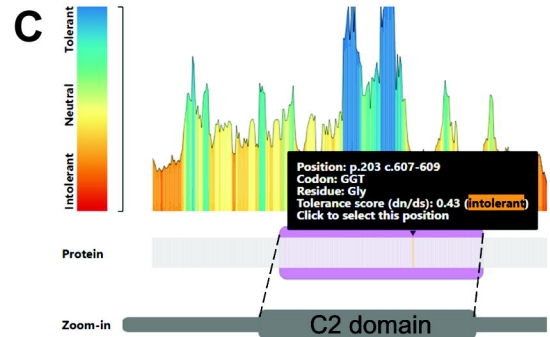


A

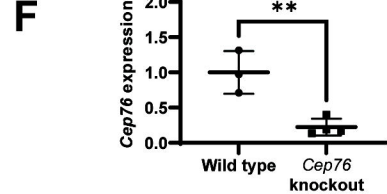
Gene	Genomic position	cDNA position	Protein position	Genotype	Allele frequency
CEP76	g.Chr18:12697322C>G	c.607G>C	p.Gly203Arg	Homozygous	0.0015%

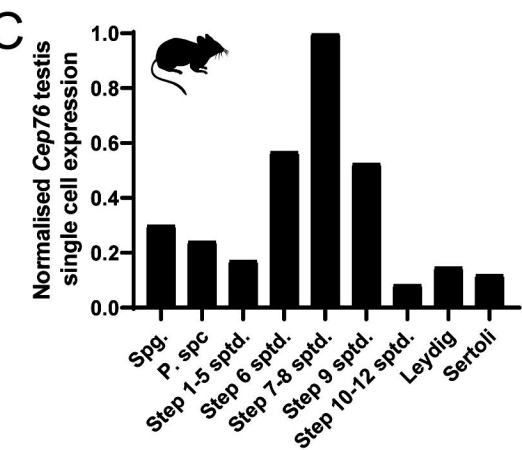
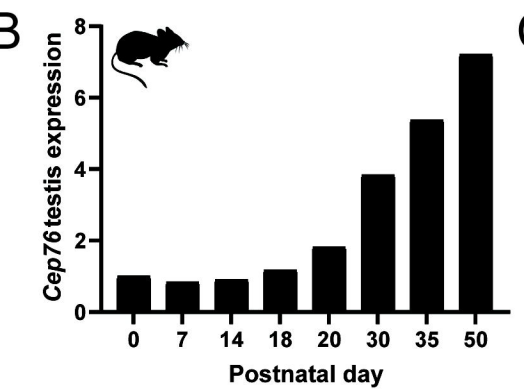
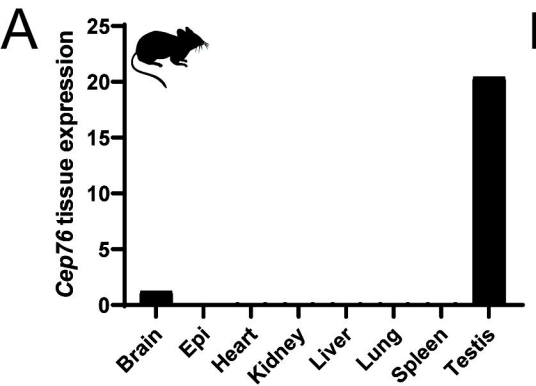
B

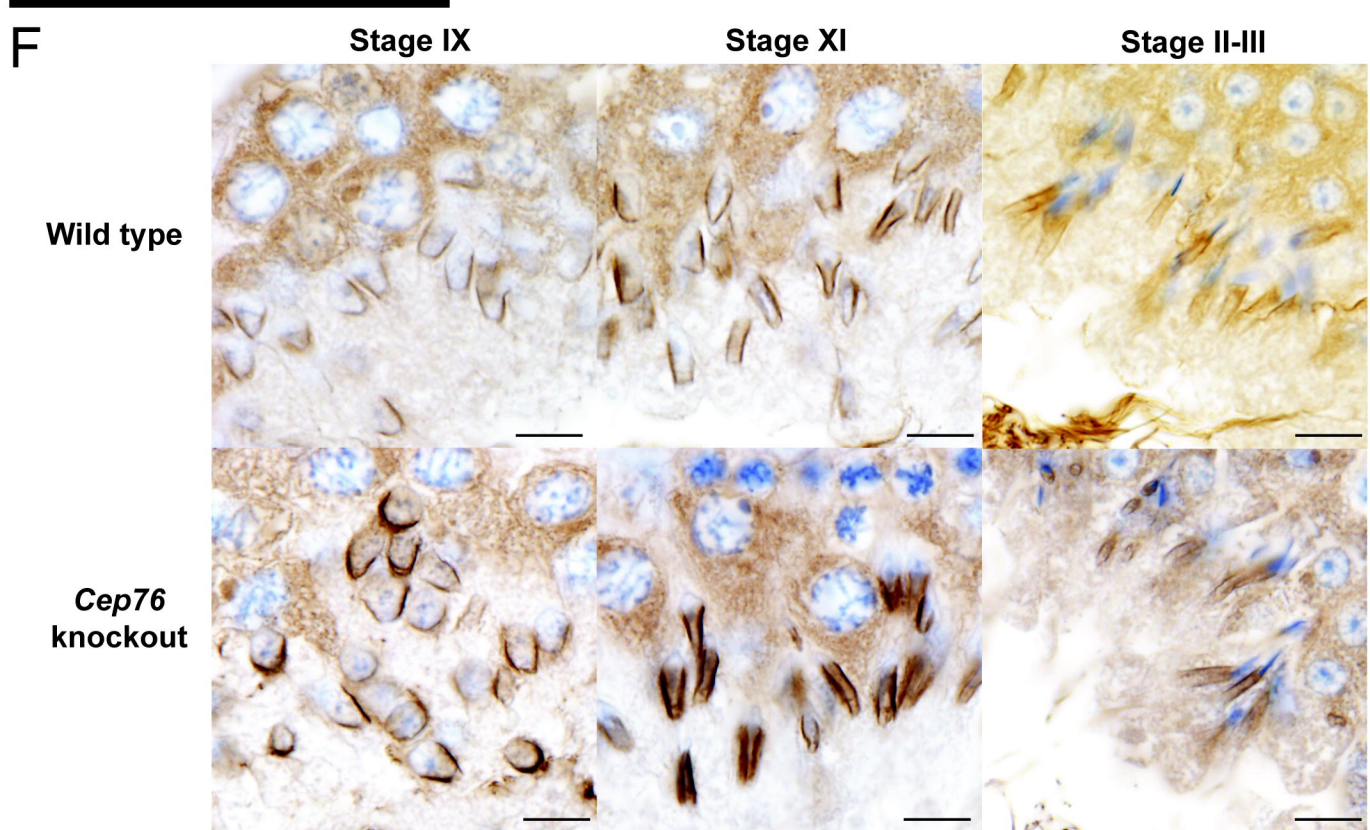
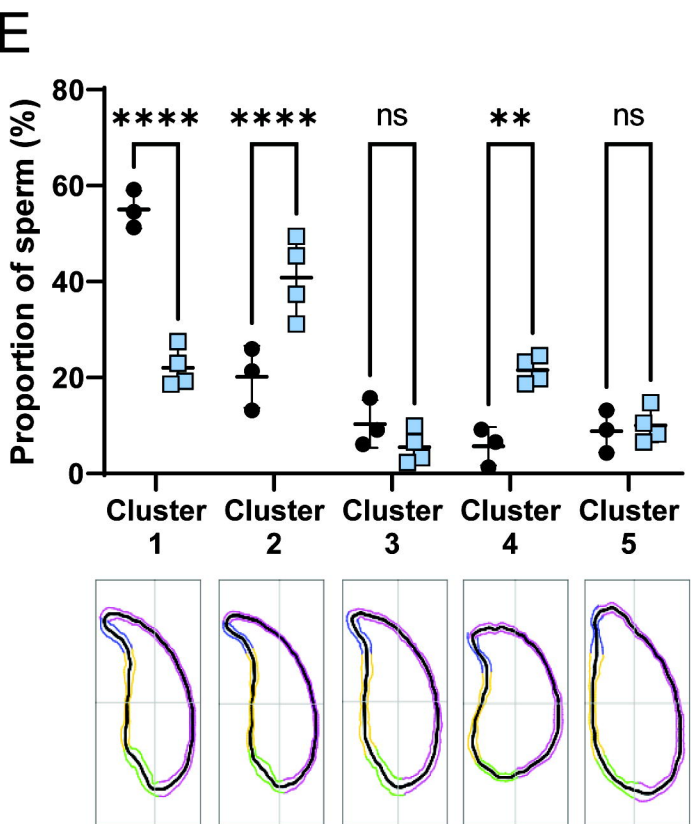
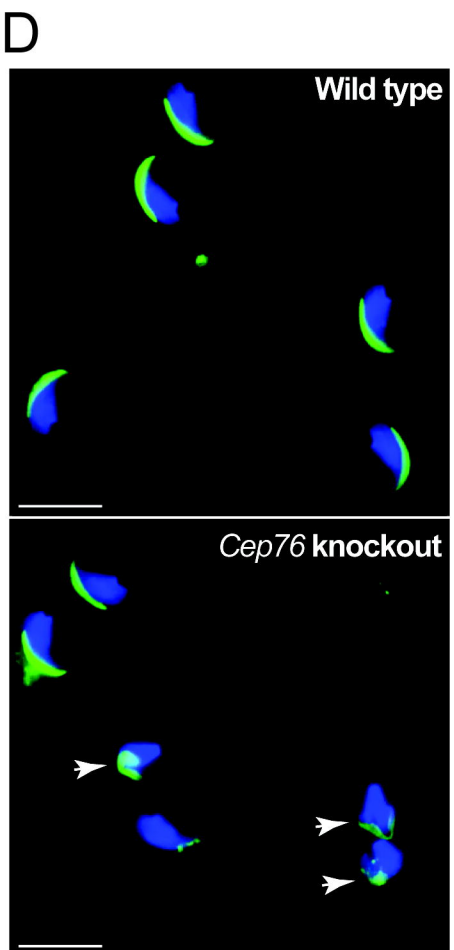
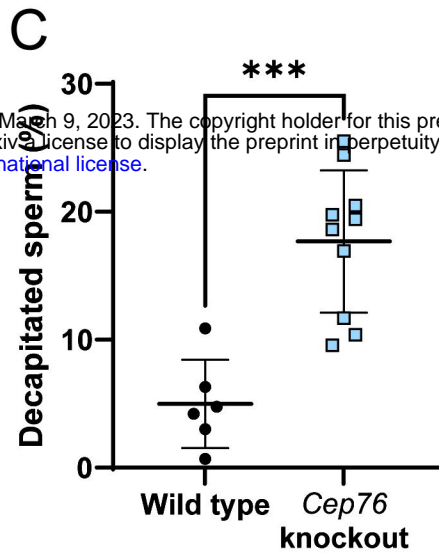
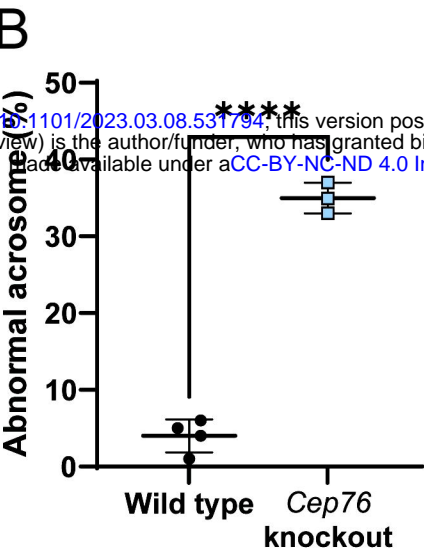
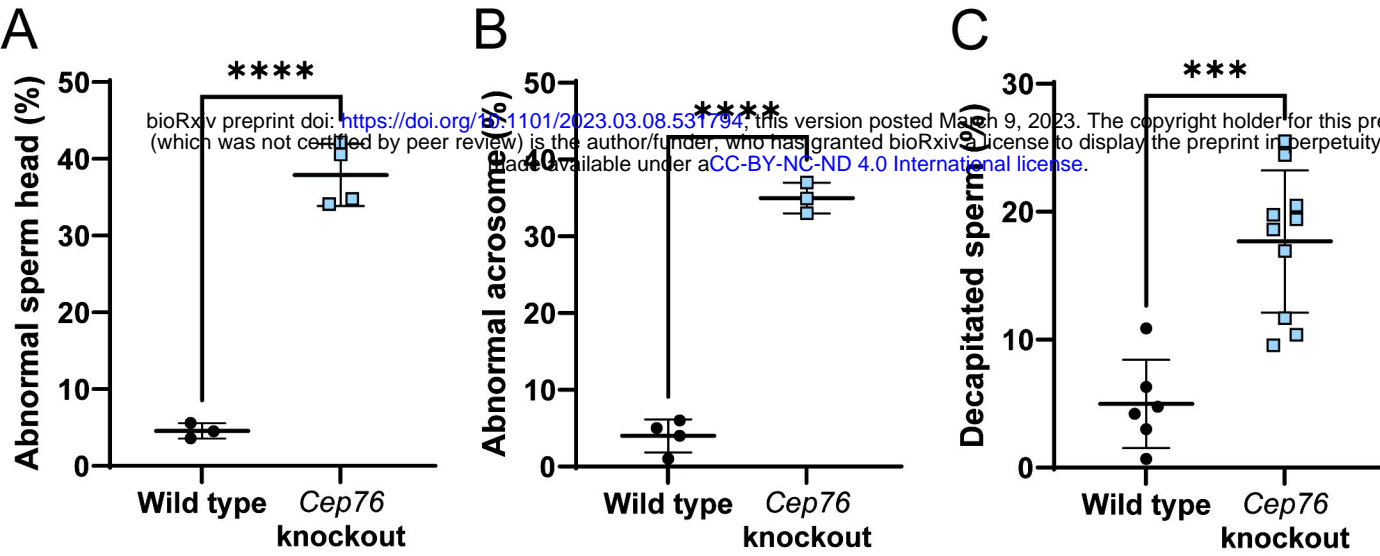
Species	Alignment	Identity
<i>Homo sapiens</i>	KTDIF <u>G</u> ETTLV	100%
<i>Infertile man</i>	KTDIF <u>R</u> ETTLV	99.8%
<i>Pan troglodytes</i>	KTDIF <u>G</u> ETTLV	99.7%
<i>Macaca mulatta</i>	KTDIF <u>G</u> ETTLV	99.5%
<i>Rattus norvegicus</i>	KTDIF <u>G</u> ETTLV	97.7%
<i>Mus musculus</i>	KTDIF <u>G</u> ETTLV	97.7%
<i>Danio rerio</i>	KTD <u>TSG</u> DTTLV	68.6%



Cep76 knockout







Wild type

Cep76 knockout

